INORGANIC CHEMISTRY FRONTIERS

REVIEW

View Article Online
View Journal

Check for updates

Cite this: DOI: 10.1039/d5qi00538h

# High-entropy alloys and oxides as catalysts for water-splitting: synthesis, characterization, applications and prospects†

Tong Wu,‡[a] Xiaoyi Zhang,‡[a] Ziyu Yang,[a] Zhilin Chen,[a] Yihao Long,[b] Liang He,*[b] Changsong Dai,*[c] Jibing Chen[d] and Hui Tang*[a]

High-entropy materials (HEMs), due to their exceptional physicochemical performance, which includes a unique electronic structure, outstanding catalytic performance, and remarkable electrochemical stability, are considered to be promising catalysts for applications such as water-splitting, underscoring their potential in electrocatalysis. Given the significant potential for their development and promising future applications for HEMs as electrocatalysts, research in this field is rapidly expanding. However, despite numerous innovative advancements, comprehensive summaries of HEMs as electrocatalysts are still lacking. This review summarizes the synthesis, characterization, and applications of HEMs in electrocatalysis. We discussed the synthesis of high-entropy catalysts from three perspectives: dry synthesis, wet synthesis, and rapid energy-based synthesis. Subsequently, the employment of advanced characterization techniques is discussed, along with electronic structure analysis and DFT calculations, to evaluate the high-entropy catalysts. Additionally, we summarized the exploration of the applications of these catalysts in electrocatalysis, focusing primarily on hydrogen evolution, oxygen evolution, and oxygen reduction. Finally, we provided a summary of the review's contents and presented insights into mechanistic research, material synthesis, applications of these, and future development prospects, with the goal of offering valuable suggestions for the future synthesis and applications of these.

Received 3rd March 2025,
Accepted 22nd April 2025

DOI: 10.1039/d5qi00538h

rsc.li/frontiers-inorganic

Published on 06 May 2025. Downloaded on 8/5/2025 11:23:10 AM.

## 1. Introduction

Traditional catalysts rely on scarce and costly noble metals, exacerbating resource depletion risks. High-entropy materials (HEMs),[1–3] including high-entropy alloys (HEAs),[4–6] high-entropy oxides (HEOs),[7–9] high-entropy metal sulfides (HEMSs),[10,11] and others, have recently garnered significant attention from researchers. Their unique electronic structures, where each atom in a HEM exists in a different coordination environment,[12] enable their use as catalysts in water splitting, fuel cells, and other applications.[13–15] These advantages position HEMs as economically viable and sustainable solutions for energy technologies, aligning with global efforts to mitigate energy scarcity and improve industrial cost-effectiveness.

The concept of high entropy was first introduced for the development of HEAs, with the earliest reports dating back to 2004.[16,17] Before this formal publication, similar materials were studied under different names.[18] Following the introduction of the high-entropy concept, these materials rapidly became a focal point of research. HEMs were found to have superior physical properties, and their catalytic potential was subsequently recognized. According to recent reports, substantial research efforts have been directed toward HEMs.[19–22] As demonstrated in Fig. 1, since being proposed in 2004, significant progress has been made in the research and development of HEMs.

HEMs exhibit remarkable physical properties, such as high strength, superior hardness, and enhanced wear resistance, as well as exceptional chemical properties like corrosion resistance, thermal stability, and catalytic activity.[23–25] The multiple components in HEMs interact to provide ligand and strain effects, influencing the d-band structure and the electronic structure of the active sites. This unique, adjustable electronic structure holds great promise in the field of catalysis.[26] The

[a]School of Materials and Energy, University of Electronic Science and Technology of China, Chengdu, 611731, China. E-mail: tanghui@uestc.edu.cn
[b]School of Mechanical Engineering, State Key Laboratory of Intelligent Construction and Healthy Operation and Maintenance of Deep Underground Engineering, Sichuan University, Chengdu 610065, P. R. China. E-mail: hel20@scu.edu.cn
[c]School of Chemistry and Chemical Engineering, Harbin Institute of Technology, Harbin 150001, P. R. China. E-mail: changsd@hit.edu.cn
[d]School of Mechanical Engineering, Wuhan Polytechnic University, Wuhan 430023, China

†Electronic supplementary information (ESI) available. See DOI: https://doi.org/10.1039/d5qi00538h

‡These authors contributed equally to this work.

Published on 06 May 2025. Downloaded on 8/5/2025 11:23:10 AM.

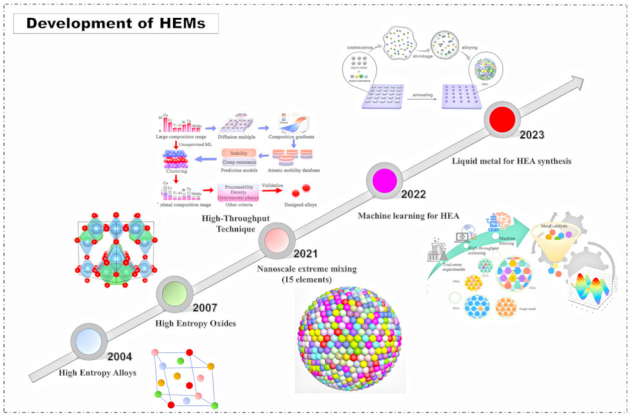


**Fig. 1** The development of HEMs (cited from refs. 23–27).

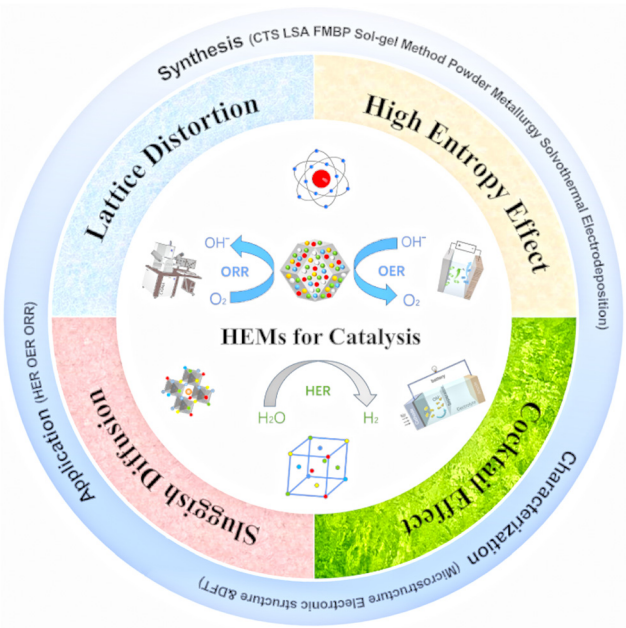


**Fig. 2** Overview of the topics covered in this review.

core characteristics of HEMs, HEAs, HEOs, and HEMSs are high configurational entropy and significant lattice distortion due to their multi-component nature.[27–29] Despite these similarities, differences exist among these materials, stemming from their distinct compositions and structural variations.

Due to their unique composition and special electronic structure, HEMs have shown great potential in energy-related applications such as water-splitting and fuel cells.[30,31] Water-splitting and fuel cells are two important fields that have a wide range of applications in energy conversion and storage, and are considered to be the core components of future clean energy systems. With the progress of green and low-carbon science and technology, as well as the maturity of the market, water decomposition and fuel cells are expected to achieve large-scale applications in the next few years, providing strong support for the global economic and social transformation to green and low-carbon.

For instance, many studies have demonstrated the superior performance of HEAs in the catalysis of the hydrogen evolution reaction (HER), the oxygen evolution reaction (OER), and fuel cells. Additionally, other types of HEMs, including HEOs and HEMSs, have shown outstanding performance in the oxygen reduction reaction (ORR) and HER/OER, respectively.[32–36] Thus, high-entropy electrocatalysts hold significant research potential and applications in new energy resources.

Recently, numerous exceptional HEMs have been employed as catalysts, exhibiting noteworthy catalytic properties in diverse reactions. Comprehensive reviews have been conducted, covering the design, synthesis, applications, and calculations of HEMs, thereby enhancing our understanding and offering guidance for further development. Building upon existing research efforts, this review presents a thorough overview of recent advancements in the synthesis of high-entropy catalysts, with a focus on practical applications.

This is achieved by examining various synthesis pathways employed for various types of HEMs and elucidating the underlying principles governing their formation. Furthermore, this review describes the distinctive characteristics exhibited by HEMs and explores their applications in water-splitting and fuel cell-related reactions (primarily HER, OER, and ORR).[37–39] Finally, an analysis of both the prospects and challenges associated with employing HEMs as catalysts is provided. The ultimate objective of this review is to offer valuable insights and guidance for synthesizing highly efficient high-entropy catalysts. And all the topics covered in this review are demonstrated in Fig. 2.

This review distinguishes itself by introducing a dry–wet rapid energy-based synthesis framework that uniquely elevates rapid energy-based synthesis as an independent category, emphasizing emerging technologies' critical role in fabricating nanoscale HEMs—a departure from conventional classifications based solely on material types or singular synthesis routes. It establishes a comprehensive research architecture for high entropy electrocatalysis through a closed-loop synthesis–characterization–application–theory analytical approach, integrating fundamental exploration with practical implementation. These original perspectives not only strengthen theoretical foundations for material research but also delineate engineering-oriented pathways, signifying a paradigm shift in HEMs from conventional fabrication toward systematic investigations encompassing precision design, advanced characterization, and scenario-specific optimization.

## 2. Fundamentals of high-entropy materials as catalysts

HEMs have remarkable structural stability, enhanced mechanical properties, and superior resistance to wear and corrosion. In the realm of catalysis, HEMs offer exciting possibilities for


This journal is © the Partner Organisations 2025

Published on 06 May 2025. Downloaded on 8/5/2025 11:23:10 AM.

developing catalysts with exceptional performance. The intricate interplay between the multiple constituent elements can lead to synergistic effects that enhance catalytic activity, selectivity, and durability. Understanding the fundamental properties and design principles of HEMs is crucial for harnessing these benefits.

### 2.1 Definition of high-entropy materials

HEMs are a class of advanced materials characterized by their unique compositional complexity and enhanced properties. The term "high-entropy" typically refers to the high configurational entropy of these materials, which arises from the significant mixing of multiple principal elements in nearly equal proportions. This concept is most commonly applied to HEAs, but it can also extend to ceramics, polymers, and other material classes.

Take HEAs for example, HEAs can be defined in two primary ways: component-based and entropy-based. The component-based definition characterizes HEAs as materials containing five or more elements in relatively high concentrations (5–35 at%).[40] In contrast, the entropy-based definition identifies HEAs through their mixed configurational entropy. While it appears more rigorous to define HEMs by configurational entropy, the component-based definition is empirical. However, the threshold for configurational entropy can vary across different multicomponent systems.[41]

The entropy-based definition identifies HEAs *via* the mixed configuration entropy ($S$). The mixed configuration entropy of HEAs is able to be depicted by the following eqn (1).

$$S = -R\sum^{\mathrm{xi}} \ln(\mathrm{xi}) \quad (1)$$

where $R$ is the molar gas constant, and xi represents the mole fraction of the elemental component.[4]

As such, $S$ of HEAs with equal molar ratios for metallic elements in the liquid state or the solid solution state can be simplified as eqn (2).

$$S = R\ln(n) \quad (2)$$

where $n$ represents the number of components in the alloy.[4]

For an alloy with the number of elemental components ≥5, the alloy with mixed configuration entropy $S \geq 1.5R$ refers to a HEA. Particularly, the alloy with $S \geq 1.36R$ is also identified as a HEA for a quaternary alloy.[19,42] These two definitions of HEAs cover a wide range of alloys based on composition and entropy, and in most cases overlap.

For oxides, configuration entropy $S \geq$ the experience threshold $1.5R$, it can be generally regarded as the formation of HEO. In addition, HEO usually exhibits entropy stability under the premise of high configurational entropy, but entropy stability is not a necessary condition. Other HEMs such as HEMS and HEPI basically refer to configuration entropies greater than or equal to $1.5R$, or entropy stability is achieved when the components are not fewer than five.[43] For example, HEMSs usually feature homogeneously mixed multimetallic elements (≥5) in a sulfide structure.[44]

In addition to the entropy value, the chemical bond properties of HEMs are also closely related. The stability of HEMs is intrinsically linked to their chemical bonding characteristics, which differ markedly between HEAs and HEOs. In HEAs, metallic bonding—defined by delocalized electron clouds and electrostatic interactions between cations and free electrons—imparts isotropic mechanical properties, high ductility, and exceptional electron mobility. This bonding underpins their structural stability, as random solid-solution phases (*e.g.*, FCC or BCC) accommodate multiple principal elements within shared lattice sites. Local lattice distortions, though significant, are mitigated by the electron cloud's ability to buffer strain energy, suppressing elemental segregation. Furthermore, the high configurational entropy ($\Delta S_{\mathrm{config}}$) of HEAs dominates their Gibbs free energy ($\Delta G = \Delta H - T\Delta S$), favoring single-phase solid solutions over intermetallic compounds at elevated temperatures. In contrast, HEOs derive stability from a hybrid bonding framework: predominantly ionic interactions between metal cations and $O^{2-}$ anions, with partial covalent contributions from high-valent cations.[45] The rigid $O^{2-}$ sublattice acts as a stabilizing scaffold, dispersing cationic lattice distortions electrostatically while maintaining structural integrity.[46] Unlike HEAs, HEOs leverage both configurational entropy and strong ionic/covalent bonding energies to offset positive mixing enthalpy ($\Delta H_{\mathrm{mix}}$), ensuring thermodynamic stability across wide temperature ranges. This synergy also grants HEOs superior corrosion resistance in $Cl^-$-rich environments, where the $O^{2-}$ sublattice effectively blocks $Cl^-$ penetration, a critical limitation for HEAs. Mechanistically, metallic bonding in HEAs prioritizes entropy-driven stabilization and mechanical resilience, whereas HEOs excel under extreme chemical/thermal conditions due to their ionic–covalent hybrid nature.[47–49] Fig. 3(a–c) gives an example of how element selection is made, and finally HEMs are obtained with outstanding stabilization.

### 2.2 Core features of high-entropy materials

HEMs possess distinctive features like high entropy, lattice distortion, sluggish diffusion, and the cocktail effect.[50–52] These characteristics significantly influence the electrocatalytic performance of HEMs, making them promising candidates for replacing traditional noble metal catalysts.

According to the Gibbs free energy equation, materials with high-entropy will experience a significant reduction in Gibbs free energy at elevated temperatures. This decrease in free energy enhances the overall stability of the system. Additionally, the high-entropy results in a disordered distribution of the constituent elements within the material, which helps to prevent phase separation.

The random distribution of multiple elements in HEMs leads to high configurational entropy, contributing to material stabilization and enhanced thermodynamic stability. The complex constituent elements and significant atomic size differences, coupled with random atomic distribution, result in internal structures that differ markedly from crystalline materials, causing severe lattice distortion.[53,54] The serious

Published on 06 May 2025. Downloaded on 8/5/2025 11:23:10 AM.

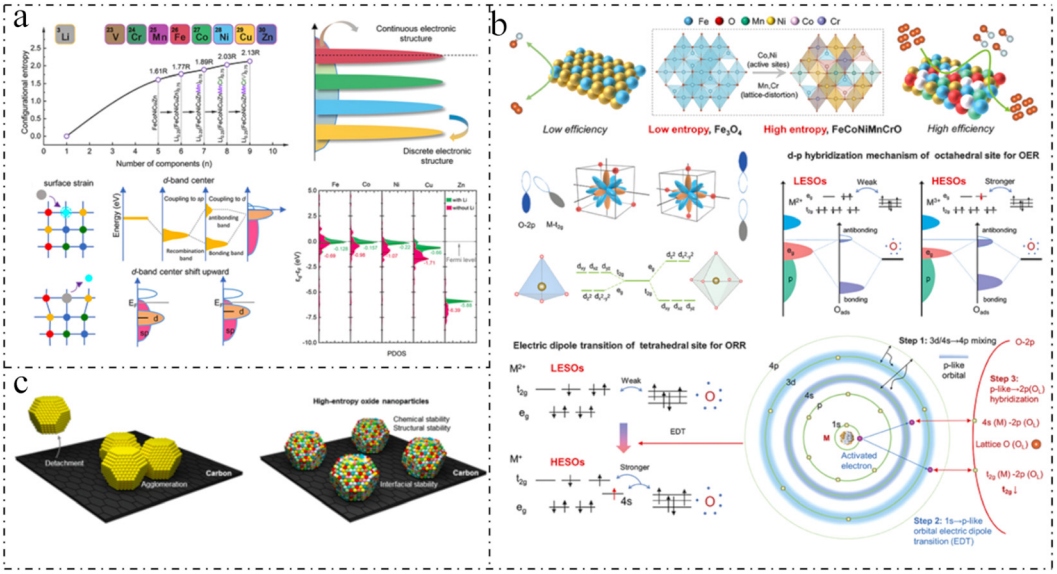


**Fig. 3** (a) Schematic diagram of elemental selection and calculations (cited from ref. 33). (b) Schematic illustrating the mechanism of high-entropy spinel oxides for decoupling oxygen reduction and evolution reactions (cited from ref. 45). (c) Carbon-supported high-entropy oxide (HEO) nanoparticles as stable electrocatalysts (cited from ref. 46).

lattice distortion in HEAs is considered for raising the energy barrier of atomic diffusion. Because of lattice distortion, mass diffusion inside the material is hindered, which also contributes to the formation of HEAs.[55,56] Compared with conventional alloys or ideal lattices, the single-phase crystals formed produce great lattice distortion, greatly changing the atomic environment of each atom, and the electronic structure is changed, thus altering the catalysis performance in various reactions.

Besides, in the high-entropy environment, the strong local electron interactions between the atoms of different elements will change the electron density and thus the catalytic activity. Due to the unique binding energy distribution, HEA nanoparticles can be readily tuned to obtain the desired surface properties for optimal catalytic performance. Interactions between different atoms and irregular atomic arrangements affect the diffusion of atoms in HEAs, with each vacancy in the lattice surrounded by a different atom. As a result, the lattice potential energy at different locations exhibits significant differences, which results in a high diffusion activation energy that inhibits the diffusion of atoms.

The "cocktail effect" in high-entropy alloys (HEAs) refers to the synergistic interplay of multiple constituent elements that collectively yield properties surpassing those of single-metal or binary systems, driven by three interlinked mechanisms: electronic structure modulation, lattice distortion-induced adsorption optimization, and multisite cooperative catalysis.[8,57] At the electronic level, the coexistence of elements with varying electronegativities and atomic radii induces charge redistribution, as exemplified by shifts in the d-band center of transition metals (*e.g.*, Ni, Fe, or Co), which directly regulates the adsorption strength of reaction intermediates (*e.g.*, *H, *O, or OOH). Concurrently, severe lattice distortions arising from atomic size mismatch generate localized strain fields and disordered coordination environments, which optimize adsorption energies by creating heterogeneous active sites with tailored binding strengths.[58] Furthermore, the multisite synergy enables parallel reaction pathways, collectively accelerating kinetics in complex reactions like overall water splitting. Such cooperative effects, absent in single-element catalysts, are further amplified by entropy-stabilized phase homogeneity, which prevents elemental segregation under operational conditions.

### 2.3 Effect of high entropy on catalyst performance

Lattice distortion and electronic state modulation in HEMs synergistically govern their catalytic activity through atomic-scale structural and electronic rearrangements. The random occupancy of lattice sites by multiple elements with varying atomic radii induces localized lattice strain, altering metal–ligand bond lengths and angles, which directly shifts the d-band center position—a critical descriptor of adsorption energetics. For instance, in HEAs, compressive strain lowers the d-band center, weakening the hydrogen adsorption energy to approach the optimal value for the HER, thereby accelerating the Volmer–Heyrovsky steps. Conversely, tensile strain in HEOs elevates the d-band center, strengthening the adsorption of oxygen-containing intermediates (*OH, *O, *OOH). Simultaneously, charge redistribution driven by electronegativity differences between constituent elements (*e.g.*, electron withdrawal from low-electronegativity metals to high-electronegativity oxygen) creates localized electron-rich/electron-deficient regions, optimizing intermediate binding. Beyond electronic effects, multisite synergy enables functional


This journal is © the Partner Organisations 2025

Published on 06 May 2025. Downloaded on 8/5/2025 11:23:10 AM.

partitioning; such spatially resolved cooperation, absent in single-element catalysts, is further enhanced by entropy-stabilized homogeneity, which prevents phase segregation under operational stress. These intertwined mechanisms—spanning atomic-scale strain, electronic tailoring, and element-specific role allocation—collectively define the superior catalytic versatility of HEMs, offering a blueprint for designing multifunctional materials beyond the limits of conventional systems.

### 2.4 Design of high-entropy materials

Due to its diverse composition and unique structure, it shows great potential in the field of catalysis. The principle and design strategy for catalytic performance improvement of catalysts with HEMs are discussed from the perspectives of composition, electronic structure, active sites, adsorption and deionization energy.

As HEMs typically consist of five or more constituent elements, the process of selecting constituent elements and adjusting the proportions of each element becomes crucial.

HEMs are usually composed of five or more elements mixed in close to equal molar ratios. This multi-alloying effect can lead to enhanced surface activity, as the synergies of different elements may provide diverse reaction paths. By changing the proportion of the elements in a HEM, it is theoretically possible to precisely adjust the physical and chemical properties of the catalyst.

In HEMs, the coexistence of multiple elements can significantly affect the density of electron states (DOS) and thus the position of the Fermi levels.[59] This helps to optimize the adsorption strength of the reactants and products and improve the catalytic efficiency. In addition, by adjusting the component elements, it is possible to design HEMs with specific band gaps or conductivity properties, thereby optimizing their performance in electrocatalysis.[60]

Moreover, due to the uneven distribution of different elements on the surface of HEAs, a large number of heterogeneous active sites will be formed, which may have higher activity and selectivity. The HEMs are prepared as nanoparticles or thin films to increase the specific surface area and improve the catalytic efficiency. Specific morphologies can also be constructed using self-assembly techniques or template methods to further enhance the catalytic activity.

The Sabatier principle posits that for a catalyst to be effective, it must have an optimal binding strength for the reactants. If binding is too weak, the reactants will not adhere to the catalyst surface long enough to react. Conversely, if binding is too strong, the reactants may not be able to desorb after the reaction, leading to catalyst deactivation.[61,62] In designing catalysts, especially for processes like hydrogenation and oxidation, understanding the Sabatier principle helps researchers select materials that can achieve the desired balance of binding energies.[63,64]

Under guidance from the volcano map, the selection of appropriate elements for catalyst synthesis helps to achieve a balance to obtain the best binding energy for improved catalytic efficiency.

## 3 Synthesis strategies for high-entropy materials

A controllable and facile synthesis method is crucial for the cost-effective preparation and widespread applications of HEMs, as it forms the foundation for large-scale utilization. To achieve superior performance, HEM catalysts are typically designed at the nanometer scale or with nanometer-level surface topography, enhancing the specific surface area and providing more active sites.

Due to the inherent multi-component nature of HEMs, a broad selection of raw materials and diverse preparation strategies are available, offering extensive flexibility in synthesis approaches. In this review, we categorize synthesis methods as dry synthesis and wet synthesis based on whether a solution system is involved in the synthesis process. Given the particularities of deposition techniques such as magnetron sputtering in dry synthesis, we further discussed dry synthesis by dividing them into sputtering and non-sputtering methods.

By examining raw material choices, the underlying principles of each synthesis method, and describing the product morphology and properties, the advantages and disadvantages of different approaches are compared. This comprehensive evaluation aims to provide an objective assessment to guide researchers in selecting appropriate methods for synthesizing high-performance HEM catalysts tailored to specific applications.

### 3.1 Dry synthesis of high-entropy materials

Dry synthesis methods, including powder metallurgy and physical vapor deposition (PVD), and many others, present numerous advantages for the fabrication of HEMs. These methods facilitate homogeneous mixing, enable controlled composition, offer scalability and versatility, and contribute to a reduced environmental impact.[65–67]

**3.1.1 Conventional dry synthesis strategy.** Powder metallurgy utilizes metal powders, or a combination of metal and non-metal powders, as the primary raw materials. Through processes such as compaction and sintering, this method facilitates the production of a diverse array of metals, composite structures, and various product forms. The synthesis of catalysts, especially HEAs, *via* powder metallurgy is often more straightforward and efficient than many conventional methods. Moreover, the specific surface area of the resultant materials can be finely tuned through techniques such as dealloying or pore formation. Importantly, powder metallurgy yields self-supporting bulk materials that exhibit enhanced stability compared with those of loose powders. When a catalyst demonstrates superior performance, it holds significant potential for practical applications across various fields. Given these advantages, powder metallurgy plays a critical role in the advancement of novel materials and addresses challenges associated with material synthesis.[68–70]

For instance, Liu *et al.* successfully synthesized a porous NiCoFeMoMn HEA exhibiting exceptional electrochemical per-

Published on 06 May 2025. Downloaded on 8/5/2025 11:23:10 AM.

formance using powder metallurgy techniques.[71] The precursor of high-entropy NiCoFeMoMn alloy ribbons was prepared by arc melting and single-roller melt spinning. The nanoporous NiCoFeMoMn catalyst was subsequently fabricated *via* a one-step electrochemical dealloying process, which significantly increased the number of active sites. This alloy demonstrated high catalytic activity for the HER and impressive efficiency for the OER in alkaline solutions. As shown in Fig. 4 (a and b), DFT calculations indicate that the effective performance of the NiCoFeMoMn alloy is attributed to the synergistic effects of the alloying elements on surface electron density between the single atom (SA) and un-SAs. This research contributes to the development of cost-effective HEA catalysts.

Besides, Chen *et al.* developed a series of oxygen micro-alloyed HEAs (O-HEAs) *via* a metallurgy approach.[72] Fig. 4c outlines the design and preparation strategy for O-HEAs, while Fig. 4d showcases island-like $Cr_2O_3$ microdomains within the HEA matrix. Fig. 4e further illustrates the electrochemical applications of various samples. Their findings revealed that a bulk O-HEA composed of $(CrFeCoNi)_{97}O_3$ exhibited a remarkable electrocatalytic performance for the OER, which was attributed to the formation of island-like $Cr_2O_3$ microdomains, leaching of $Cr^{3+}$, and structural amorphization at the interfaces of these domains.

In addition to melting and subsequent treatment such as cutting and corrosion after mixing the metal powder directly, mechanical alloying through ball milling during the mixing process represents a viable strategy. Liu *et al.* employed multi-stage mechanical alloying to construct nanocrystalline $FeCoNiCr_{0.4}Cu_{0.2}$ HEA powders characterized by large aspect ratios and thin intergranular amorphous layers.[73] Although this product was not utilized for electrocatalysis, its uniform element distribution, excellent manufacturability, and the ability to adjust the crystal phase and crystallinity through varying grinding times provided a valuable approach for preparing high-entropy catalysts.

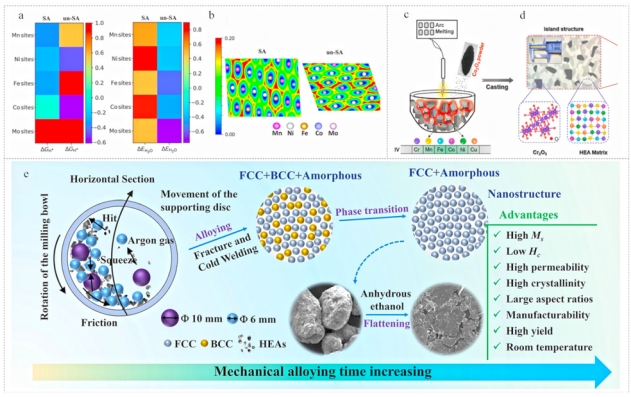


**Fig. 4** (a) Colored $\Delta G_{H^*}$ and $\Delta E_{H_2O}$ comparisons of SA and un-SA. (b) The ELF maps of SA and un-SA (cited from ref. 72). (c) Atomic-level design and the preparation process for the O-HEA electrode. (d) Multilevel structure of the O-HEA integrated electrode. The inset shows the size of the bulk O-HEA electrode (cited from ref. 73). (e) Multistage mechanical alloying strategy and microstructure design concept (cited from ref. 74).

**3.1.2 Deposition and magnetron sputtering.** In addition to powder metallurgy, the growth of high-entropy catalysts *via* vapor deposition or sputtering represents another promising avenue in dry synthesis. Vapor deposition, a sophisticated manufacturing process, is employed to create thin films or coatings of alloys onto various substrates. In this process, alloy source materials are heated to a high temperature within a vacuum chamber, causing them to evaporate or sublimate and subsequently condense onto the substrate. Alternatively, sputtering involves bombarding a target material with high-energy ions, leading to the ejection of atoms from its surface. This method allows for precise control over alloy composition, microstructure, and thickness, thereby tailoring material properties to specific needs. Such controllability in material manufacturing is advantageous for designing and producing high-entropy catalysts aimed at enhancing performance and stability.

For instance, Wang *et al.* successfully deposited HEA thin films on carbon fiber cloth using pulsed DC reactive magnetron sputtering.[74] As illustrated in Fig. 5a, prior to deposition, the target was cleaned by $Ar^+$ bombardment to remove surface impurities. Subsequently, FeCoNiCuPd HEA thin films were deposited onto the carbon fiber cloth through pulsed DC reactive magnetron sputtering of Fe/Co/Ni/Cu targets.

In a related study, Chida *et al.* proposed an experimental platform enabling the vacuum synthesis of atomic-level-controlled single-crystal HEA surfaces.[75] This platform provides indispensable insights into understanding the microstructural intricacies crucial for electrocatalysis. Specifically, it elucidates the complex interplay between surface microstructures of multi-component alloys and their catalytic behaviors (Fig. 5b).

The dry synthesis methods discussed above offer robust pathways for fabricating advanced high-entropy catalysts with tailored properties suited to specific applications. These methodologies not only ensure homogeneous mixing controlled composition but also enhance environmental sustainability, making them invaluable tools for advancing the field of electrocatalysis beyond traditional boundaries.

### 3.2 Wet synthesis of high-entropy materials

In the synthesis of high-entropy catalysts, solution-based methods are predominantly used due to their less stringent experimental requirements compared with dry synthesis, allowing for milder synthesis conditions. Techniques such as solvothermal, MOF (metal–organic framework), and sol–gel methods are widely employed in the preparation of HEMs or their precursors within solution systems. By adjusting parameters such as the solution composition, reaction temperature, and reaction time, researchers can control the material's properties including composition, dispersion, and morphology to achieve enhanced catalytic performance.

**3.2.1 Conventional wet synthesis strategy.** As shown in Fig. 6(a and b), Gu *et al.* synthesized high-entropy layered


This journal is © the Partner Organisations 2025

Published on 06 May 2025. Downloaded on 8/5/2025 11:23:10 AM.

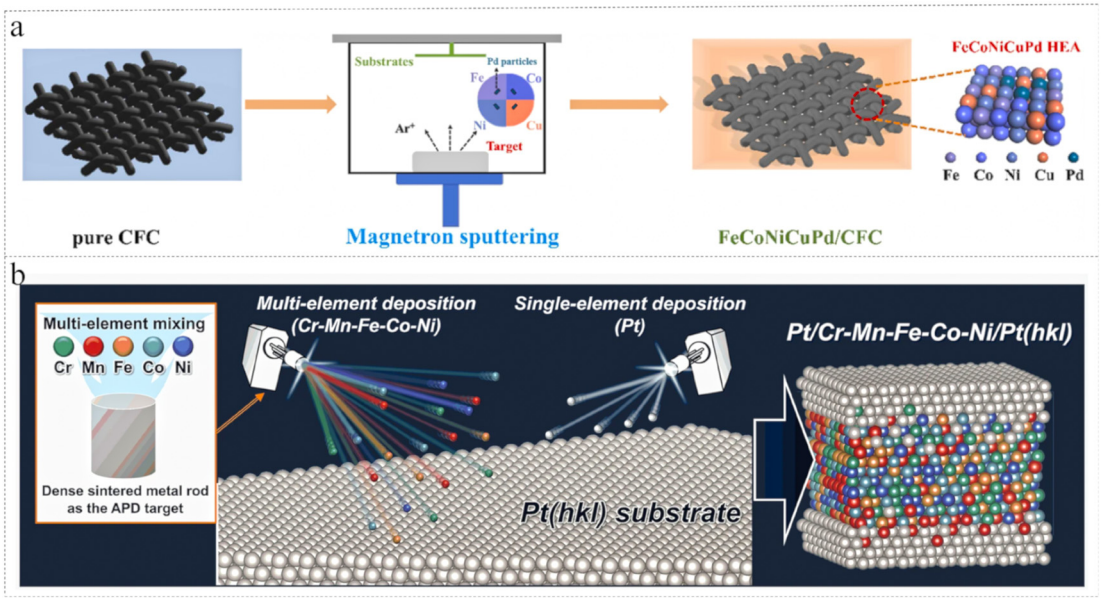


**Fig. 5** (a) Schematic illustration of key FeCoNiCuPd thin film fabrication steps (cited from ref. 75). (b) Schematic illustration of the experimental study platform of the HEA electrocatalysis model surface (cited from ref. 76).

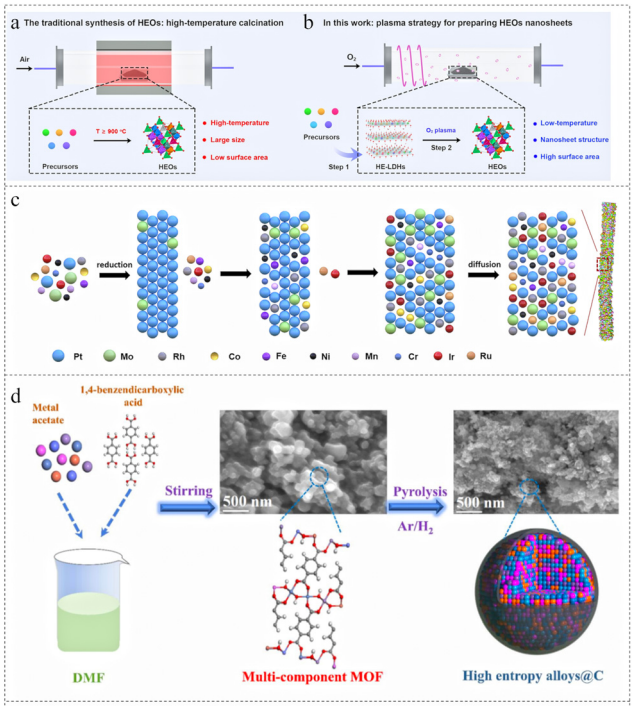


**Fig. 6** (a) The traditional synthesis method and (b) the low-temperature plasma strategy for HEOs (cited from ref. 77). (c) Schematic showing the formation process for 10-HEA NWs (cited from ref. 78). (d) Schematic illustration of the electrocatalyst preparation steps (cited from ref. 79).

double hydroxides (LDHs) using a one-step hydrothermal method.[76] To obtain the quinary $(FeCrCoNiCu)_3O_4$ nanosheets, the precursors were treated with oxygen plasma. This plasma treatment preserved the nanosheet structure while creating abundant surface oxygen vacancies and a high specific surface area, effectively improving the electrocatalytic activity.

In addition to hydrothermal and solvothermal methods, which are also commonly employed for synthesizing high-entropy catalyst precursors, Sun *et al.* synthesized a series of Pt-based high-entropy metallic nanowires *via* a solvothermal method as demonstrated in Fig. 6c.[77] This technique uniformly mixes multiple elements at low temperatures (180–220 °C), forming high-entropy nanowires with controllable structures and compositions. It can be extended to the preparation of 17 types of high-entropy nanowires. Compared with their low-entropy counterparts, lattice distortion in these nanowires alters the strain distribution and electronic structure, exhibiting excellent catalytic performance in the hydroxide oxidation reaction (HOR) and the HER.

By heating precursors in a solvent at low temperatures, it is possible to synthesize stable nanoparticles with small particle sizes that are well dispersed.[78,80,81] Adjusting the heating time and temperature along with solution components allows for tuning of the crystal morphology, size, pore size, and functionalization degree; this is a significant advantage over melting methods that struggle with nanoscale preparation. This is a good solution to the shortcomings of melting and other methods that are difficult to use to prepare nanoscale materials, so it can be used for the preparation of nanoscale catalysts.

Building on solvothermal methods, coating metal precursors with organic frameworks offers another convenient approach for preparing high-entropy catalysts. Fan *et al.*, for instance, synthesized MOF precursors on carbon cloth *via* solvothermal techniques followed by thermal treatment under a reducing atmosphere to obtain HEA catalysts.

Published on 06 May 2025. Downloaded on 8/5/2025 11:23:10 AM.

However, the solvothermal process is not always necessary, Wang *et al.* reported an easy-to-scale method for synthesizing advanced HEA (CoNiCuMnAl)/C nanoparticles from polymetallic MOFs.[82] As shown in Fig. 6d, the MOF precursor of the catalyst was obtained by fully stirring the organometallic salt and the organic ligand in the solvent and forming a precipitate during the reaction. The face-centered cubic structure of the HEA core was coated in an ultra-thin carbon shell and deposited on Ni foam, exhibiting a superior OER performance.

The sol–gel method can achieve molecular-level homogeneity in a very short time. During the formation of the gel, the reactants are likely to be evenly mixed at the molecular level.[79] Due to the solution reaction step, it is easy to uniformly and quantitatively incorporate certain elements, resulting in uniform doping at the molecular level. This is beneficial for synthesizing high-entropy catalysts. Additionally, the sol–gel method requires only a low synthesis temperature and it is generally believed that component diffusion in the sol–gel system occurs at the nanometer scale. Thus, the reaction proceeds easily and requires relatively low temperatures for synthesis.

Using this method, Tang *et al.* synthesized a high-entropy perovskite cobaltate consisting of five equimolar metals (Mg, Mn, Fe, Co, and Ni) in the B-site as an electrocatalyst for the OER,[83] as shown in Fig. 7(a and b). The high-entropy cobaltate demonstrates a low overpotential, outperforming its other counterparts.

While synthesizing HEO particles *via* the sol–gel method is straightforward and feasible, special consideration must be given to prevent agglomeration of oxides during reduction when synthesizing HEAs. As demonstrated in Fig. 7c, Kwon *et al.* synthesized an Ir-based electrocatalyst, which was designed based on the HEA platform ZnNiCoIrX with two elements (X: Fe and Mn) and prepared by the sol–gel method.[26] Instead of reducing oxide powder produced by the gel directly, they annealed nitrate gels under a flow of $H_2$/Ar gas to avoid potential agglomeration during annealing.

In addition, ion exchange is currently a widely used method for preparing high-entropy catalysts. Miao *et al.* developed a ZnFeNiCuCoRu–O HEO catalyst that exhibited exceptional activity and ultra-stability for the OER over the full pH range *via* ion exchange.[84] Their synthesis strategy involves using a MOF as a template to create HEO catalysts with polyhedral shapes and hollow structures, incorporating up to 10 different metal elements. This approach underscores the significance of the ion-exchange method for producing highly stable and active hollow-structured HEO catalysts, which are crucial for efficient energy conversion and storage devices.

**3.2.2 Rapid energy-based synthesis of high-entropy materials.** In addition to the methods introduced by conventional wet synthesis and adjusting the solution system and reaction conditions, another synthesis strategy involves forcing the precursor to transform into the target high-entropy catalyst by altering the energy source output during synthesis.

Carbothermal shock is a facile method for synthesizing multi-metal nanoparticles, including HEM nanoparticles (HEM-NPs). In this approach, the preparation involves loading metal precursors onto a conductive carrier, such as a carbon substrate. Once prepared, the carrier is connected to a power source, and nanoparticles are generated by running a short pulse of electrical current through the sample to raise the temperature instantaneously. The rapid rise and fall in temperature during carbothermal shock make it an innovative way to synthesize nanoparticles.

Yao *et al.* synthesized extreme HEA nanoparticles containing 15 elements using carbothermal shock.[85] Fig. 8a demonstrates that their method involves Joule heating of precursor-loaded carbon nanofiber films. By adhering to alloying criteria and employing high-entropy designs coupled with high temperatures, they achieved a record 15-element HEA nanoparticle. This process overcame immiscibility in strongly repulsive combinations and induced metal reduction of easily oxidized elements, thereby extending the range of synthesizable HEAs and demonstrating the great potential of HEMs. Similarly, Abdelhafiz *et al.* synthesized a type of non-noble metal HEO catalyst *in situ* on carbon fiber through rapid Joule heating and quenching.[86] Their synthesis protocol started with drop-casting multi-metal chloride salts dissolved in ethanol at a concentration of 50 mM onto carbon fiber paper. Quenching occurred within fractions of a second, forming solid HEA nanoparticles.

Laser ablation is a surface modification technique where cladding material is added to the surface of the substrate, which is irradiated by a laser beam with a high energy density. This process forms a cladding layer on the substrate's surface that is metallurgically bonded and exhibits special physical, chemical, or mechanical properties through rapid melting,

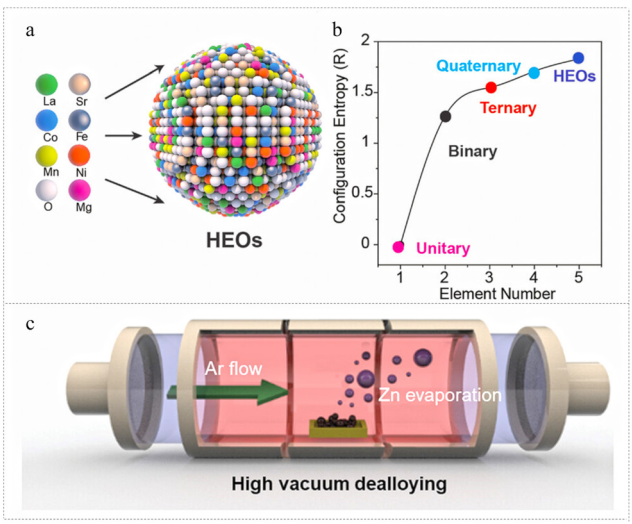


**Fig. 7** (a) Schematic demonstrating the structure of high-entropy perovskite oxide nanoparticles with uniformly dispersed elements. (b) Configurational entropy as a function of the number of cations in the B-site in the material system (cited from ref. 83). (c) Schematic illustration of selective Zn dealloying through a vapor dealloying process (cited from ref. 31).


This journal is © the Partner Organisations 2025

Published on 06 May 2025. Downloaded on 8/5/2025 11:23:10 AM.

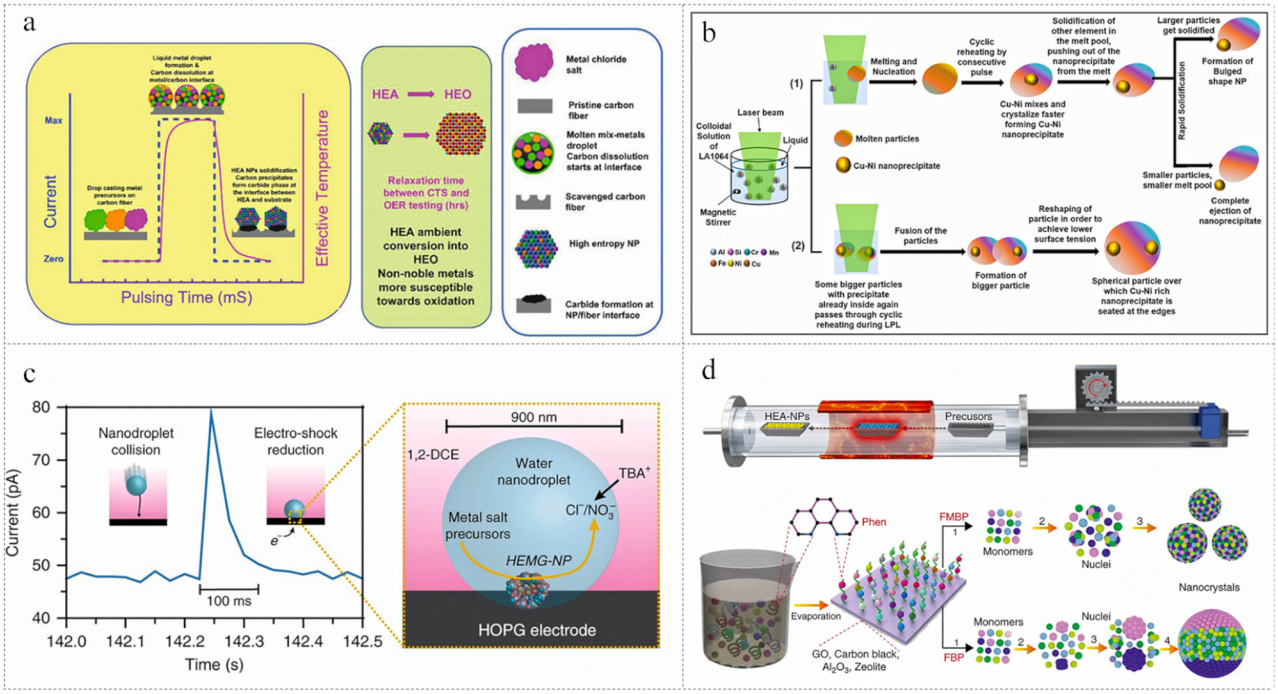


**Fig. 8** (a) Schematic showing the ultra-fast rapid Joule heating and spontaneous cooling process within mS pulse intervals (cited from ref. 25). (b) Schematic showing the mechanism of morphological changes in LP532 (cited from ref. 87). (c) Nanodroplet-mediated electrodeposition overview for controlling NP stoichiometry and microstructure (cited from ref. 88). (d) The FMBP strategy for the synthesis of HEA-NPs (cited from ref. 89).

expansion, and solidification. The cladding layer has a low dilution rate, fewer pores, good metallurgical bonding with the matrix, and properties such as high hardness, good corrosion resistance, wear resistance, and stable quality. As presented in Fig. 8b, Rawat *et al.* synthesized Al-rich non-equiatomic HEA NPs by ablating the $Al_{40}(SiCrMnFeNiCu)_{60}$ (at%) target in deionized water.[87] This work investigated and discussed structural, compositional, and morphological changes in $Al_{40}(SiCrMnFeNiCu)_{60}$ NPs, and put forward a possible formation mechanism for Cu–Ni enriched HEA NPs. Besides, Wang *et al.* synthesized a library of HEA and ceramic nanoparticles by laser scanning ablation.[90] Their work presented an easy-to-adopt strategy for developing HEA and HEC NPs.

The electrochemical deposition method involves connecting the power supply to the anode and cathode poles of the electrolyte to form a circuit in a water-soluble or organic-soluble electrolyte. Under the influence of an electric field, an electrochemical reaction occurs, causing ions to precipitate as dense pure metals or alloys onto a substrate through a redox reaction, thereby creating the desired coating. This method avoids high temperatures during synthesis, making it a relatively straightforward synthesis strategy. For example, Glasscott *et al.* presented a generalized strategy to electro-synthesize HEMG-NPs with up to eight equimolar components by confining multiple metal salt precursors in water nanodroplets emulsified in dichloroethane.[91] As shown in Fig. 8c, HEMG-NPs were electrodeposited on highly ordered pyrolytic graphite (HOPG) or glassy carbon substrate electrodes from a water-in-oil emulsion system.[88] Additionally, Chang *et al.* developed a high-entropy FeCoNiMnW alloy *in situ* on carbon paper using a pulsed current electrodeposition method.[92]

In previously used synthesis methods like carbothermal shock and electrochemical shock, these methods required conductive carriers, which limited carrier selection significantly. Gao *et al.*, based on the common wet impregnation method, proposed a fast-moving bed pyrolysis (FMBP) approach for synthesizing HEA nanoparticles (HEA-NPs).[89] In this work, a facile FMBP synthesis strategy was developed for HEA-NPs with up to ten elements by ensuring mixed precursors were pyrolyzed at high temperatures simultaneously. This resulted in highly dispersed HEA-NPs on supports, as detailed in Fig. 8d.

These methods outlined above highlight the versatility and efficiency of rapid energy-based synthesis techniques for producing advanced HEMs with potential applications in catalysis, coatings, and other fields requiring superior material properties. Finally, the synthesis methods mentioned above are summarized in Table 1.

Overall, the synthesis of HEMs faces inherent limitations tied to method-specific constraints. Solid-state approaches like powder metallurgy and magnetron sputtering suffer from high equipment costs, nanomaterial scalability challenges, and impurity incorporation (*e.g.*, sputtering gases), which can be mitigated *via* cost-effective sintering alternatives, high-purity targets, or reactive gas optimization. Vapor-phase techniques (PVD, electrodeposition) struggle with weak film–substrate adhesion and slow deposition rates, necessitating interfacial engineering (*e.g.*, adhesion layers) or pulsed electrodeposition

Published on 06 May 2025. Downloaded on 8/5/2025 11:23:10 AM.

Table 1 Summary of synthesis methods

| Synthesis method | Advantage | Limitation | Applicable scope |
|---|---|---|---|
| Powder metallurgy | Precise composition control; high mechanical stability; tunable porosity *via* post-sintering dealloying/etching | High equipment cost; challenges in nanomaterial synthesis | High-strength bulk catalysts for high-temperature reactors |
| PVD | Ultra-thin film uniformity; precise thickness control | Weak film–substrate adhesion at elevated temperatures; high cost | Ultrathin catalytic coatings |
| Magnetron sputtering | High-density films; scalable deposition | Impurities from sputtering gases or low-purity targets; target consumption | Nanoscale multilayer films |
| Hydrothermal | High crystallinity; synthesis of metastable phases (*e.g.*, spinel HEOs) | Batch size limitation (<100 mL); high-pressure reactor required | Phase-pure HEOs |
| Solvothermal | Size-controlled nanoparticles; excellent dispersion | Toxic/organic solvents; high cost | HEA NPs |
| MOF | Ultrahigh surface area; atomic-level dispersion | Low stability in non-carbonized forms; complex synthesis | Porous carbon composite catalyst |
| Sol–gel | Molecular homogeneity; low-temperature processing; mesoporous structures *via* supercritical drying | Time-consuming drying; gel shrinkage | 150 nm |
| Ion-exchange | Tailored morphologies (*e.g.*, hollow/core–shell structures) | Impurity risks; strict condition control | Synthesis of catalyst with specific morphology |
| Carbon thermal shock | Ultrafast synthesis (<1 s); immiscible metal integration | Limited to conductive substrates (*e.g.*, carbon cloth); small-scale only | HEA NP libraries for high-throughput HER/OER screening |
| Laser ablation | Purity >99.9%; ligand-free surfaces; colloidal NP synthesis | Low yield; high energy consumption | HEA |
| Electrochemical deposition | Atomic-level thickness control (*e.g.*, monolayer deposition); ambient conditions | Slow deposition rates (improved *via* pulsed techniques) | Corrosion-resistant coatings, microelectronic interconnects |
| Fast-moving bed | Ultra-fine powders; instant precursor aerosolization and pyrolysis | Lab-scale only; precise atmospheric control required | Ultrafine HEOs |

protocols. Solution-based methods (hydrothermal, solvothermal, MOF-derived) are hindered by batch size restrictions, toxic solvents, and instability in non-carbonized forms; scalable reactors, green solvent alternatives, and hybrid carbonization strategies offer promising solutions. Emerging methods such as carbothermal shock and laser ablation are limited by substrate dependency and low yields, requiring substrate versatility (*e.g.*, ceramic supports) or energy-efficient pulsed modulation. Techniques like sol–gel and flash pyrolysis demand accelerated drying processes (*e.g.*, microwave-assisted supercritical drying) and precise atmospheric control to minimize gel shrinkage and phase inhomogeneity. Cross-method synergies—*e.g.*, integrating ion exchange's morphology control with electrodeposition's atomic precision or coupling MOF-derived confinement with flash pyrolysis—could unlock tailored catalytic architectures. Future advancements should prioritize scalable, energy-efficient protocols with *in situ* characterization to resolve metastable phase dynamics, ensuring industrial viability for applications in energy conversion, environmental catalysis, and high-throughput systems.

# 4 Characterization and calculation of high-entropy materials

The influence of each component element on the electronic structure of HEMs is crucial for determining the selection of active sites during catalytic processes, directly impacting their catalytic performance. The microstructure of these materials dictates their specific surface area and adsorption capabilities, significantly influencing their catalytic efficacy.[93–95] In the characterization and analysis of HEMs, the complexity introduced by multiple constituent elements poses significant challenges. While basic characterization methods can determine and confirm morphology, composition, and electronic states, their limited resolution often hampers the ability to decouple contributions from individual elements accurately. Therefore, advanced high-precision techniques are essential for gaining a comprehensive understanding of atomic arrangement, bonding coordination, and electronic properties in high-entropy nanoparticles. Traditional methods struggle to correlate electronic structure characteristics with compositional and structural data effectively. To address this challenge, DFT calculations are introduced as a powerful tool for analyzing the electronic structure and energy characteristics of HEMs. DFT provides insights into atomic arrangements, bonding interactions, and coordination environments that influence electrochemical properties. This computational approach helps elucidate underlying reaction mechanisms and identify active sites responsible for observed catalytic activity.[96–98]

## 4.1 Composition structure analysis for high-entropy materials

Given that HEMs primarily consist of single solid solutions characterized by disordered atomic arrangements and a uniform distribution of constituent elements, traditional characterization methods such as X-ray diffraction (XRD), X-ray photoelectron spectroscopy (XPS), energy-dispersive X-ray spec-


This journal is © the Partner Organisations 2025

Published on 06 May 2025. Downloaded on 8/5/2025 11:23:10 AM.

troscopy (EDS), and scanning electron microscopy (SEM) can elucidate the phase structure, basic chemical composition, valence states of each element, and microscopic morphology of the material.[99–102] However, constrained by their limited spatial resolution, surface sensitivity, and lack of atomic-scale resolution, these traditional methods fall short of probing the distribution and binding of atoms at the atomic level. They are unable to definitively discern the formation of a high-entropy environment within materials. Consequently, more advanced characterization techniques have become imperative for a comprehensive analysis.

Atomic electron tomography (AET) and atom probe tomography (APT) are advanced analytical techniques used for investigating the atomic-level structure and composition of materials. AET, based on transmission electron microscopy (TEM), captures a series of 2D projection images of a sample from multiple angles, which are then reconstructed into a 3D representation using computational algorithms. It provides atomic-scale spatial resolution, enabling a detailed analysis of nanostructures, interfaces, and crystal defects. APT, on the other hand, utilizes field evaporation of atoms from the sample surface in a high electric field, with a time-of-flight mass spectrometer (TOF-MS) detecting the evaporated ions. This technique allows for the 3D reconstruction of the sample's atomic arrangement and provides precise elemental composition at the atomic level. Both techniques are pivotal in materials science, particularly in the study of nanomaterials, alloys, semiconductors, and catalytic systems.

For instance, as shown in Fig. 9a, to further investigate the surface composition and understand the mechanisms of activation and deactivation of the Cantor alloy during the OER, atom APT was employed to analyze the elemental distribution and composition of the surface oxides following 70, 150, and 2000 CV cycles. The results indicate that the Cantor alloy electrocatalyst surface exhibits its most OER-active state after the 70th cycle, a slightly deactivated state after the 150th cycle, and becomes inactive after 2000 cycles.[103] APT provides a precise visualization of the arrangement of constituent elements in high-entropy catalysts, including their spatial distribution, atomic coordination, and potential atomic-scale defects or interfaces within the catalyst. Due to complex alloying and segregation behaviors at the atomic level in high-entropy catalysts, which typically consist of multiple elements in near-equiatomic compositions, APT is particularly valuable for resolving these intricate structural details.

Four-dimensional scanning transmission electron microscopy (4D-STEM) extends traditional STEM by incorporating additional dimensions related to the electron angular distribution scattering. This technique simultaneously captures both spatial and angular information about electron scattering in a sample. One key advantage is its ability to capture dynamic processes and time-resolved phenomena at the nanoscale. By acquiring sequential diffraction patterns over time, researchers can observe structural changes, phase transitions, and dynamic events in real-time.

Fig. 9e showcases an atomically resolved high-angle annular dark-field scanning transmission electron microscopy (HAADF-STEM) image of a singular 15-component high-entropy alloy nanoparticle with an accompanying 4D-STEM dataset acquired for this particle.[85] Each pixel corresponds to a diffraction pattern used to derive local structural information such as lattice constants and strain deformation. The resultant Bragg vector map indicates single crystallinity with an FCC structure at the single-particle level. By combining high spatial resolution with the capability to capture dynamic processes,

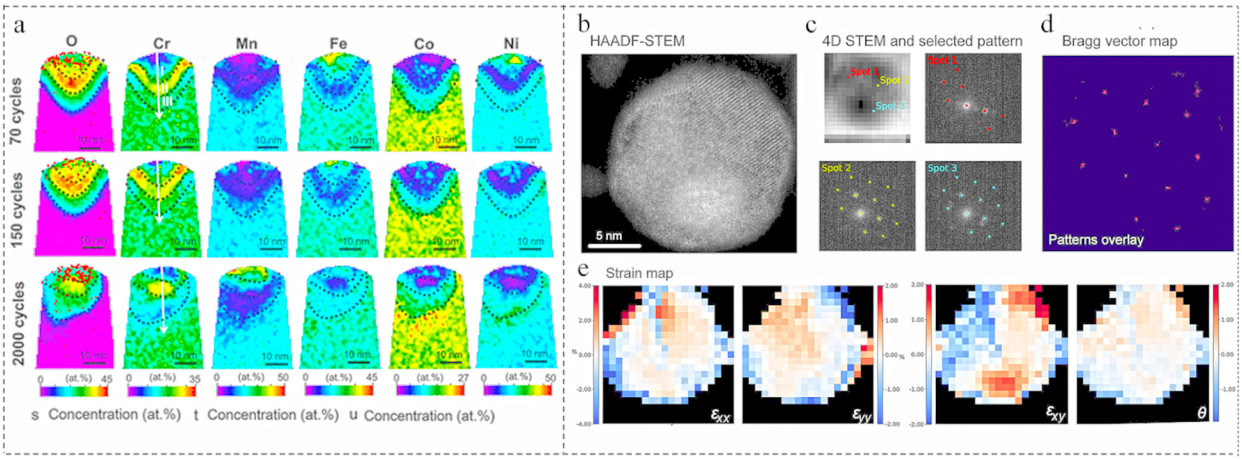


**Fig. 9** (a) 2D concentration profiles of O, Cr, Mn, Fe, Co, and Ni plotted from a 5 nm thick slice of APT data of the Cantor alloys after 70, 150, and 2000 CV cycles under OER conditions (cited from ref. 103). (b) High-magnification HAADF-STEM image of a 15-HEA nanoparticle, on which a 4D-STEM dataset of this particle was acquired. (c) Subsequently generated virtual ADF image in which each pixel corresponds to a diffraction pattern. Three selected diffraction patterns at various locations within this particle are shown. (d) Bragg vector map showing an overlay of all diffraction patterns within the particle. (e) Strain map of the 15-HEA nanoparticle calculated from the variation in the lattice, showing the localized strain and inhomogeneity in the nanoparticle due to extreme mixing (cited from ref. 25).

Published on 06 May 2025. Downloaded on 8/5/2025 11:23:10 AM.

4D-STEM offers valuable insights into the material's structure, properties, and behavior at the nanoscale.

Besides all the characterization methods mentioned above, Su *et al.* visualized the entire formation process for a high-entropy fluorite oxide from a polymeric precursor using atomic-resolution *in situ* gas-phase scanning transmission electron microscopy.[104] This approach provides a reference for exploring growth processes and formation mechanisms while aiding better design strategies for synthesizing high-entropy catalysts.

### 4.2 Electronic structure analysis of high-entropy materials

Testing electronic structures is crucial for understanding how a material's composition influences its electronic characteristics and catalytic performance.

X-ray absorption near edge structure (XANES) and extended X-ray absorption fine structure (EXAFS) are spectroscopic techniques utilizing synchrotron radiation sources to probe local atomic structures and electronic environments at the atomic scale.[105,106] As demonstrated in Fig. 10(a–i), these techniques provide detailed coordination environment information that is essential for advancing our understanding of material applications across diverse scientific fields.

Hard X-ray photoelectron spectroscopy (HAXPES) is an advanced analytical technique that probes the electronic structure of materials using high-energy X-rays. Unlike traditional XPS, which typically utilizes soft X-rays with energies up to a few keV, HAXPES employs hard X-rays with energies ranging from tens to hundreds of keV. This higher energy enables deeper penetration into the material, allowing for the study of buried interfaces and bulk properties with enhanced sensitivity and resolution.

As illustrated in Fig. 10(j and k), HAXPES can reveal detailed electronic structures such as valence bands and d-band centers in high-entropy nanoparticles.[12] These insights are closely related to the adsorption and binding energies of key reaction intermediates, helping to rationalize their catalytic activity.[107]

### 4.3 Density functional theory calculations on high-entropy materials

Density functional theory (DFT) calculations are powerful computational methods used in materials science, condensed matter physics, chemistry, and related fields to study the electronic structures, properties, and behavior of atoms, molecules, and solids.[108,109]

For instance, to understand the fundamental mechanism behind enhanced HER catalytic activity, Wang *et al.* conducted DFT calculations on the basal plane of a catalyst. The geometry was optimized using refined PXRD data.[110] As shown in Fig. 11 (a–d), their results demonstrated that the enhanced HER activity in high-entropy $MPCh_3$ originated from the synergistic effects of abundant active sites provided by the high-entropy strategy. Optimized sulfur sites on the edge and phosphorus sites on the basal plane offer more active sites for hydrogen adsorption. Additionally, manganese sites introduced on the edges act as efficient centers for water dissociation.

Similarly, Li *et al.* applied periodic DFT calculations to explore the HER and the methanol oxidation reaction (MOR) performances in HEAs.[111] As shown in Fig. 11(e–k), they compared the projected density of states (PDOS) of HEAs with slightly different stoichiometries and found highly similar electronic structures. This indicates that slight variations in HEA stoichiometry have a minimal effect on their electronic structure. By comparing different atomic arrangements, they identified an HEA structure with a slightly nickel- and copper-enriched surface as the most stable lattice model. This model exhibited subtle distortion after relaxation, which was indicative of good durability for electrocatalysis. Moreover, adsorption studies revealed active electron transfer from HEA to water and methanol during HER and MOR processes respectively, ensuring stable adsorption and facilitating subsequent reactions. The existence of a linear correlation between the transformation of intermediates throughout the MOR process, which ensured optimal binding strength and superior MOR performance in HEAs.

DFT calculations have become indispensable for deciphering the catalytic mechanisms of HEMs, bridging atomic-scale electronic interactions with macroscopic performance. At the core of this understanding lies electronic structure modulation, where DFT reveals how compositional complexity tailors catalytic behavior. To address HEMs' vast compositional space, DFT synergizes with machine learning (ML) by

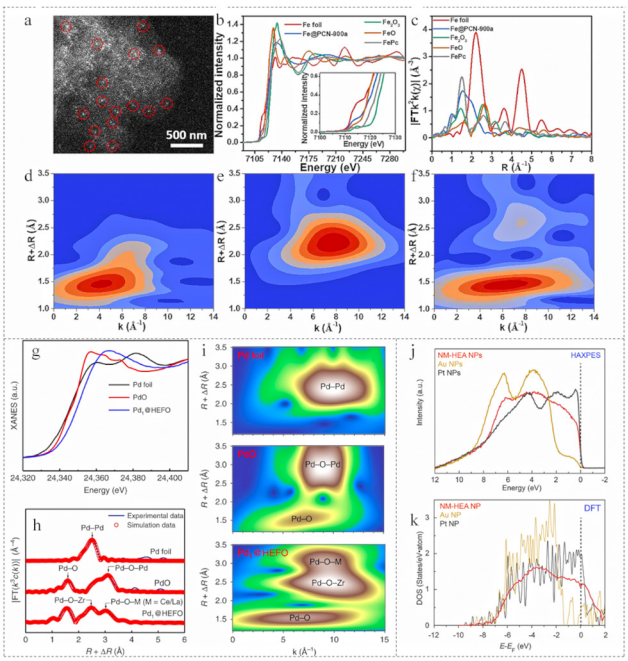


**Fig. 10** (a) HAADF-STEM image of Fe@PCN-900a. (b) Normalized Fe K-edge XANES spectra and (c) EXAFS spectra of Fe@PCN-900a, FePc, Fe foil, FeO and $Fe_2O_3$. Wavelet transform of Fe K-edge EXAFS of (d) Fe@PCN-900a, (e) Fe foil and (f) FePc (cited from ref. 106). (g) XANES spectra at the Pd K-edge. (h) The *k*3-weighted Fourier transforms of Pd K-edge EXAFS spectra, and (i) wavelet transforms from experimental data for Pd1@HEFO, PdO, and Pd foil (cited from ref. 105). (j) VB spectra obtained by HAXPES and (k) DOS profiles calculated by DFT for the NPs of NM-HEA, Pt, and Au (cited from ref. 12).


This journal is © the Partner Organisations 2025

Published on 06 May 2025. Downloaded on 8/5/2025 11:23:10 AM.

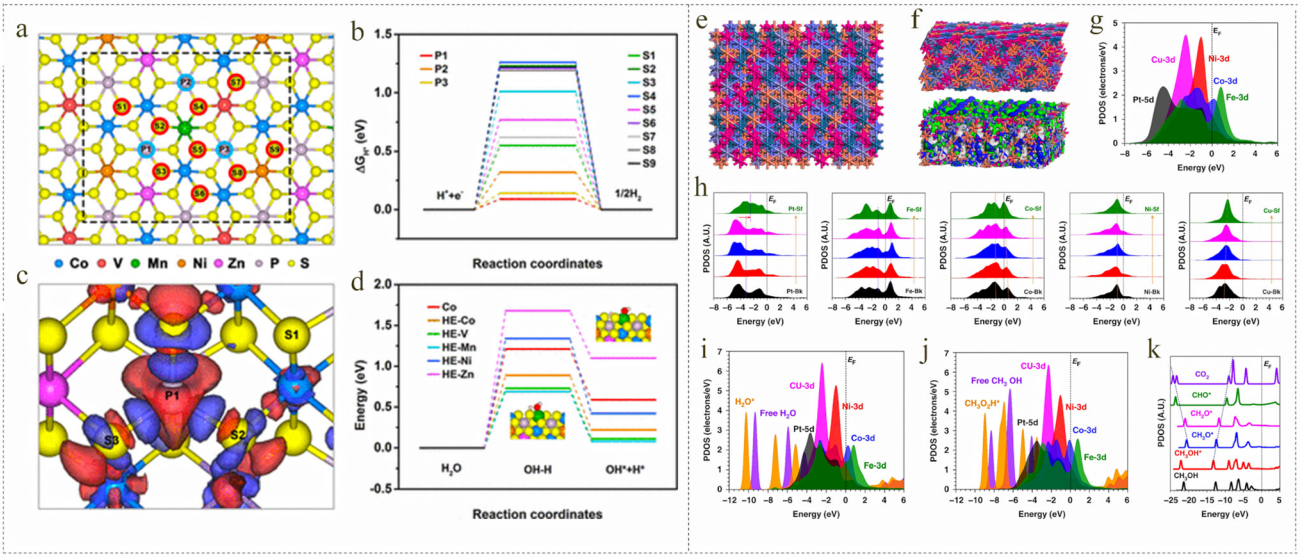


**Fig. 11** (a) Basal-plane models of P sites (P1–P3) and S sites (S1–S9) in $Co_{0.6}(VMnNiZn)_{0.4}PS_3$. (b) HER free-energy diagram of corresponding sites in (a). (c) Calculated charge-density difference of the P1 site for $Co_{0.6}(VMnNiZn)_{0.4}PS_3$. The red and blue regions refer to electron accumulation and depletion, respectively. (d) Calculated reaction energy of water dissociation for $Co_{0.6}(VMnNiZn)_{0.4}PS_3$ and $CoPS_3$, including Co, V, Mn, Ni, and Zn sites (cited from ref. 110). (e–k) Density functional theory calculations for the structural configuration and PDOSs (cited from ref. 111).

providing datasets (*e.g.*, formation energies, adsorption descriptors) that train ML models to predict phase stability and screen optimal compositions. For example, ML models trained on DFT-calculated d-band centers and metal–oxygen bond strengths accelerate the discovery of OER-active HEOs. However, challenges persist in modeling metastable phases and dynamic surface reconstructions under operational conditions, necessitating advanced *ab initio* molecular dynamics (AIMD) and hybrid functional approaches. By integrating electronic insights, active site hierarchies, and reaction energetics, DFT not only decodes HEMs' catalytic superiority but also guides the rational design of next-generation catalysts for energy conversion and storage.

Overall, DFT has enabled researchers to elucidate the electronic structures of the catalysts synthesized effectively. Moving forward, it will play an even greater role in guiding catalyst design and synthesis.

# 5 The electrochemical performance of high-entropy materials

In the fields of new energy, water splitting has garnered significant attention. Key reactions, such as HER, OER, and ORR, play crucial roles in these technologies. The rate of these reactions and their energy utilization efficiency significantly impact the overall efficiency and application prospects of fuel cells and water splitting systems.

## 5.1 Hydrogen evolution reaction

The HER is a multi-step process that is often sluggish due to kinetic limitations.[112] The mechanism of the HER can generally be divided into two main types of step: the adsorption step (Volmer step) and desorption steps.[113,114]

In the adsorption step, protons ($H^+$) are transferred from solution to the surface of the electrode and adsorbed on it, while electrons are transferred from the electrode to the proton.[115] Desorption steps involve two possible paths:[116] (1) the Tafel step (hydrogen–hydrogen recombination mechanism); two adsorbed hydrogen atoms combine to form hydrogen gas; and (2) the Heyrovsky step (proton–electron coupling transfer mechanism); an adsorbed hydrogen atom combines with a proton and an electron to form hydrogen gas.

In acidic media, the HER usually follows the mechanism described above, while in alkaline media, the difference is that the proton donor is obtained by the dissociation of water molecules, due to the extremely low proton concentration in alkaline media. Obviously, the HER mechanism in alkaline electrolytes is much more complex than in acidic electrolytes. Thus, the corresponding electrocatalytic kinetics of the HER is two to three orders of magnitude slower than that of acid media.[117]

Therefore, electrocatalysts with outstanding catalytic performances are essential to enhance HER efficiency.[118–120] Currently, the HER primarily utilizes Pt-based precious metal catalysts because of their low overpotentials and high exchange current density.[121,122] Among these, Pt/C is the most widely used catalyst for the HER. However, the scarcity and high cost of noble metals limit the widespread applications of Pt-based electrocatalysts. Thus, exploring alternative catalysts such as HEMs becomes significant.

As shown in Fig. 12a, Gu *et al.* reported a Turing structuring strategy to activate and stabilize superthin metal nanosheets by incorporating high-density nanotwins, which synergistically reduced the energy barrier of water dissociation and optimized

Published on 06 May 2025. Downloaded on 8/5/2025 11:23:10 AM.

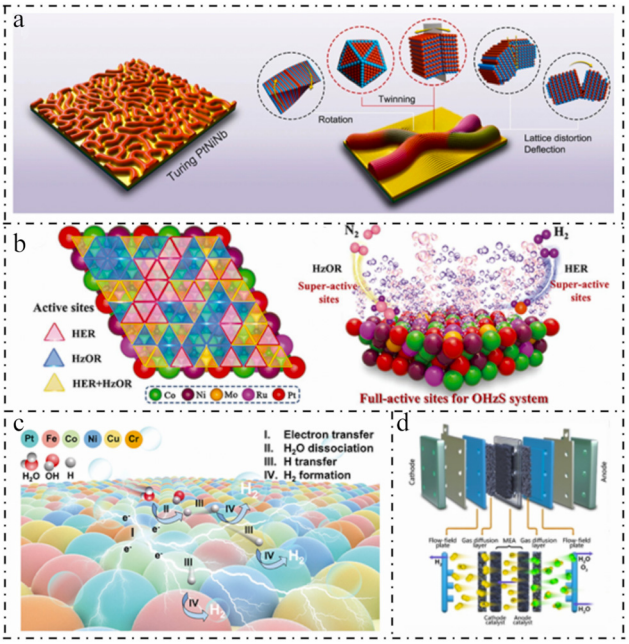


**Fig. 12** (a) Schematic diagram of the prepared Turing PtNiNb and corresponding crystallographic characterization (cited from ref. 123). (b) Schematic illustration of the full-active-site catalytic mechanism of HEANCs for the overall OHzS system (cited from ref. 124). (c) Schematic diagram of the multi-site synergistic effect in PtFeCoNiCuCr@HCS for efficient HER (cited from ref. 125). (d) Schematic diagram of the PEMWE electrolyzer (cited from ref. 126).

the hydrogen adsorption free energy for the hydrogen evolution reaction.[123]

Regarding non-noble metal high-entropy catalysts, Li *et al.* developed a quaternary FeCoNiCu HEA through dealloying the HEA, which was used as a water-splitting electrocatalyst.[124] In alkaline electrolytes, this self-supported HEA-derived porous electrode exhibited a superior HER performance with a low overpotential of 42.2 mV to achieve a current density of 10 mA $cm^{-2}$, along with a low Tafel slope of 31.7 mV $dec^{-1}$. Additionally, it demonstrated excellent stability under a high current density of 500 mA $cm^{-2}$. In this work, the synergistic effect of polymetallic atoms optimizes the HER performance through the following mechanisms: first, the alloying of Fe, Co, Ni with Cu reconstructs the coordination environment, effectively modulating the d-band electronic structure of Cu sites, which reduces the H* adsorption energy barrier and optimizes the HER kinetic process. Specifically, strong electron coupling between the s-orbitals of Cu and H near the Fermi level significantly lowers the energy barrier during H* reduction. Meanwhile, the d-orbitals of Fe/Co/Ni contribute greater electronic state density, further refining the electronic structure of active sites through orbital hybridization. This polymetallic synergy ultimately reduces both the water molecule adsorption energy and the Gibbs free energy of H* adsorption, establishing a more favorable reaction pathway for the HER.

For noble metal-based high-entropy catalysts, notable work has shown that they can approach or even exceed the catalytic performance of commercial Pt/C for the HER while reducing the amounts of precious metals required. Xia *et al.* synthesized an HEANC/C catalyst that achieved an ultrahigh mass activity of 12.85 A $mg^{-1}$ noble metals at −0.07 V and an overpotential of only 9.5 mV for achieving 10 mA $cm^{-2}$ in the alkaline HER.[125]

In the HEANC system, Pt and Ru atoms exhibit electron-rich states, while Ni and Co atoms with lower electronegativity transfer electrons to Pt/Ru sites, inducing a pronounced electron redistribution effect. This electronic structure modulation effectively optimizes the d-band center position, not only creating abundant active sites for the HER but also significantly reducing the reaction energy barrier. Fig. 12(b–d) further reveals the catalytic mechanism and active sites of the HER, demonstrating the actual process taking place during the reaction. Experimental data reveal that the system demonstrates a superior water adsorption energy ($E_{ad}$ ($H_2O$)) during the Volmer step and more favorable hydrogen adsorption free energy ($\Delta G_{H^*}$) in the Tafel step compared to pure Pt surfaces. Notably, the super-active sites exhibit $\Delta G_{H^*}$ values approaching 0 eV, which remarkably enhance the adsorption–desorption kinetics of hydrogen intermediates.

In Table 2, we provide a comparison and analysis of other recent high-entropy catalysts for the HER (unless otherwise specified, overpotential is always relative to a current of 10 mA $cm^{-2}$).

### 5.2 Oxygen evolution reaction

The OER is a four-electron–proton coupling reaction that requires high energy, resulting in a higher overpotential than the theoretical decomposition voltage of water (1.23 V).[142–144] Designing and synthesizing efficient OER catalysts are crucial for improving the efficiency of hydrogen production through water electrolysis. Currently, the most effective OER catalysts are oxides of precious metals such as iridium ($IrO_2$) and ruthenium ($RuO_2$).[145–147] However, their scarcity and high cost limit their large-scale applications, prompting the search for alternatives. The specific catalytic mechanism of the OER is demonstrated in Fig. 13(a–c), revealing the reaction steps and the adsorption and desorption of intermediate reactants.

HEMs provide a promising path to discover new OER catalysts beyond noble metals. For example, Wang *et al.* prepared FeCoNiPB, FeCoPB, FeNiPB, and CoNiPB nanomaterials using a one-step chemical reduction method.[151] The ORR efficiency of FeCoNiPB, containing three transition metals, was compared with samples containing two transition metals. In 1.0 M KOH solution, FeCoNiPB achieved a current density of 10 mA $cm^{-2}$ at an overpotential of 235 mV, superior to those of FeCoPB (285 mV), FeNiPB (261 mV), CoNiPB (330 mV), and commercial $RuO_2$ (316 mV).

Notably, at a high current density of 100 mA $cm^{-2}$, FeCoNiPB maintained a low overpotential of 306 mV, better than most reported electrocatalysts. The mass activity of the FeCoNiPB catalyst was also impressive at 1983 mA $mg^{-1}$ at 1.7 V *vs.* RHE, significantly higher than FeCoPB (441 mA $mg^{-1}$), FeNiPB (1334 mA $mg^{-1}$), CoNiPB (786 mA $mg^{-1}$), and $RuO_2$


This journal is © the Partner Organisations 2025

Published on 06 May 2025. Downloaded on 8/5/2025 11:23:10 AM.





**Table 2** Summary of high-entropy catalysts for HER

| Name | Synthesis method | Morphology | Size | Tafel slope | Overpotential | Electrolyte | Ref. |
|---|---|---|---|---|---|---|---|
| $Pt_{18}Rh_{16}Mo_{15}Ir_{11}Co_9Ru_6Fe_6Mn_5Cr_5$ HEA NWs | Reduction–diffusion | Nanowire | N.A. | N.A. | 24 mV | 0.1 M KOH | 77 |
| FeCoNiCu | Metallurgy and dealloying | Porous | 12.2 nm | 31.7 mV $dec^{-1}$ | 42.2 mV | 1 M KOH | 124 |
| FeCoNiCuPd | Magnetron sputtering | Film | 2 mm thick | 47.2 mV $dec^{-1}$ | 29.7 mV | 1 M KOH | 74 |
| PdPtCuNiP | Flexible as-spun and dealloying | Nanosponge-like architecture | Less than 10 nm | 37.4 mV $dec^{-1}$ | 32 mV | 1 M KOH | 126 |
| PdFeCoNiCu/C | Oil-phase synthesis | Particle | About 30 nm | 39 mV dec-1 | 18 mV | 1 M KOH | 127 |
| np-12HEA | Powder metallurgy | Porous | 5–10 nm (grain size) | 29.5 mV $dec^{-1}$ | 21 mV | 1 M KOH | 128 |
| P doped $Ni_{30}Co_{30}Cr_{10}Fe_{10}Al_{18}W_2$ | Powder metallurgy | Porous | N.A. | 32.6 mV $dec^{-1}$ | 70 mV | 1 M KOH | 129 |
| Pt(Co/Ni)MoPdRh | Solvothermal | Nanoflower | N.A. | 26.8 mV $dec^{-1}$ | 16.5 mV | 1 M KOH | 130 |
| CoZnCdCuMnS@CF | Hydrothermal | Nanowire | N.A. | 98.5 mV $dec^{-1}$ | 173 mV | 1 M KOH | 131 |
| CoFeNiCrMnP/NF | Electrodeposition | Nanosheet | N.A. | 48 mV $dec^{-1}$ | 51 mV (100 mA $cm^{-2}$) | 1 M KOH | 132 |
| CuAlNiMoFe | Alloying/dealloying | Nanoporous Monolithic | About 400 nm | ≈60 mV $dec^{-1}$ | 56 mV (100 mA $cm^{-2}$) | 1 M KOH | 133 |
| np-UHEA14 | One-step dealloying | Nanoporous ribbons | 30–40 mm thick and 2 mm wide | 30.1 mV $dec^{-1}$ | 32 mV | 0.1 M $HClO_4$ | 134 |
| NiCoMoPtRu HEANC | Co-reduction and annealing | Nanoclusters | 1.48 nm | 29.8 mV $dec^{-1}$ | 9.5 mV | 1 M KOH | 125 |
| ZnNiCoIrMn | Sol–gel and dealloying | Spherical nanosheets | ~200 nm | 30.6 mV $dec^{-1}$ | 50 mV (50 mA $cm^{-2}$) | | 26 |
| $Pt_{28}Mo_6Pd_{28}Rh_{27}Ni_{15}$ NCs | Wet chemistry | N.A. | N.A. | 25.9 mV $dec^{-1}$ | 9.7 mV | 1 M KOH | 135 |
| IrPdPtRhRu HEA NPs | One-pot polyol process | Nanoparticles | 5.5 ± 1.2 nm | N.A. | 25 mV | 1 M KOH | 136 |
| $Pt_4FeCoCuNi$ | Impregnation | Nanoparticles | 5 nm | 31 mV $dec^{-1}$ | 20 mV | 1 M KOH | 137 |
| $Ni_{14}Co_{14}Fe_{14}Mo_6Mn_{52}$ | One-step dealloying and melting and single-roller melt spinning | Nanoporous HEA foil | ~200–300 nm | 29 mV $dec^{-1}$ | 14 mV, 150 mV (1000 mA $cm^{-2}$) | 1 M KOH | 71 |
| FeCoNiAlTi HEI | One-step chemical dealloying | N.A. | N.A. | 40.1 mV $dec^{-1}$ | 88.2 mV | 1 M KOH | 138 |
| $Co_{0.6}(VMnNiZn)_{0.4}PS_3$ | Traditional solid-state reaction and ultrasonic peeling | Nanosheets | ~400–500 nm | 65.5 mV $dec^{-1}$ | 65.9 mV | 1 M KOH | 110 |
| FeCoNiMnRu | Electrospinning technique and graphitization process | Nanoporous particles | 14.2 ± 9.1 nm | N.A. | 71 mV (100 mA $cm^{-2}$) | 1 M KOH | 139 |
| NiCoFePtRh NP | Co-reduction | Nanoporous particles | ~1.68 nm | 30.1 mV $dec^{-1}$ | 27 mV | 0.5 M $H_2SO_4$ | 140 |
| PtCoNiRuIr | High-temperature liquid shock | Nanoporous particles | ~3.24 nm | 34.2 mV $dec^{-1}$ | 18 mV | 0.5 M $H_2SO_4$ | 141 |
| $Pt_{18}Ni_{26}Fe_{15}Co_{14}Cu_{27}/C$ | Oil phase | Nanoparticles | ~3.4 nm | 30 mV $dec^{-1}$ | 11 mV | 1 M KOH | 111 |

This journal is © the Partner Organisations 2025

Published on 06 May 2025. Downloaded on 8/5/2025 11:23:10 AM.

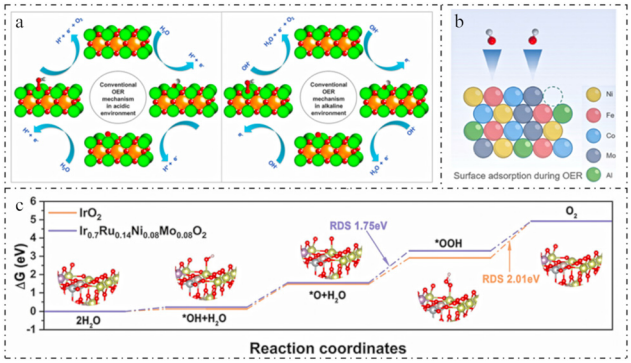


**Fig. 13** (a) Conventional OER mechanism involving proton and electron transfers on the surface metal centers (cited from ref. 148). (b) Schematic comparison of the OER mechanism over the surface of FeCoNiAlMo high-entropy alloy (cited from ref. 149). (c) Free energy diagrams of the OER at $U$ = 0 and 1.23 V on $Ir_{0.7}Ru_{0.14}Ni_{0.08}Mo_{0.08}O_2$ and $IrO_2$ models (cited from ref. 150).

(218 mA $mg^{-1}$). Analysis after 40 h of oxygen evolution showed that self-reconstruction ensured its high efficiency and stable catalytic performance during the OER.

The catalyst establishes a moderately oxidized surface microenvironment through the coexistence of metallic ($Fe^0$, $Co^0$, $Ni^0$) and oxidized states ($Fe^{2+}/Fe^{3+}$, $Co^{2+}/Co^{3+}$, $Ni^{2+}/Ni^{3+}$), providing abundant active sites for the OER. Nonmetallic B and P engage in directional electronic interactions with the metals; B donates electrons to Fe/Co/Ni, while P withdraws electrons from the metals. This synergistic electronic effect optimizes the d-band center position, reduces the adsorption free energy of *OOH intermediates, and lowers the OER overpotential. Concurrently, B/P doping enhances the amorphous phase formation capability, with the disordered structure regulating the surface adsorption behavior. During prolonged OER operation, the catalyst undergoes self-reconstruction; initial nanoparticles gradually transform into layered architectures, with edges developing highly active (FeCoNi)OOH crystalline domains. This reconstructed surface exposes numerous coordinatively unsaturated sites; $Fe^{3+}$ in reconstructed (FeCoNi)OOH acts as the primary active center, with its orbital electron occupancy approaching the ideal value, thereby enhancing the lattice oxygen-mediated (LOM) pathway efficiency.

Additionally, Qiao *et al.* synthesized a high-entropy phosphate catalyst (HEPi), specifically CoFeNiMnMoPi, which demonstrated superior catalytic activity for the OER.[152] The HEPi catalyst achieved an overpotential of 270 mV at 10 mA $cm^{-2}$, significantly lower than both its HEO counterpart (350 mV) and the benchmark $IrO_x$ catalyst (340 mV). Moreover, this HEPi catalyst can be applied to other reactions as well. Their synthesis strategy is efficient and straightforward, offering a new approach to discover various polyanionic materials for energy and catalysis applications.

In Table 3, we compare other recent high-entropy catalysts for the OER alongside those already described to provide further insights into their performance metrics (unless otherwise specified, overpotential is always relative to a current of 10 mA $cm^{-2}$).

### 5.3 Oxygen reduction reaction

The ORR is an important electrochemical conversion process in metal–air batteries and proton exchange membrane fuel cells, and the development of cost-effective catalysts with improved electrocatalytic activity and stability is crucial for promoting practical applications.[167–169] However, the multi-step nature and slow electron transfer associated with the ORR result in a low mass transfer efficiency, leading to sluggish kinetics that significantly hinders its application in practical devices. Oxygen can be reduced to hydrogen peroxide ($H_2O_2$) *via* a 2-electron pathway ($O^2 + 2H^+ + 2e^- \rightarrow H_2O_2$) or to water ($H_2O$) *via* a 4-electron pathway ($O_2 + 4H^+ + 4e^- \rightarrow 2H_2O$). The 4-electron pathway is generally preferred due to its greater reaction kinetics and efficiency.[170–172]

To address these challenges, He *et al.* synthesized FeCoNiMoW HEA nanoparticles using a solution-based low-temperature approach.[173] Linear sweep voltammetry (LSV) curves obtained from FeCoNiMoW at various rotation rates (ranging from 400 to 2500 rpm) show that at 1600 rpm, the half-wave potential is 0.71 V with an onset potential of 0.83 V. In the FeCoNiMoW catalytic system, the hybridization between Ni 3d orbitals and O 2p orbitals generates new bonding orbitals, leading to a significant reduction in anti-bonding orbital electron occupancy and increased electron density in bonding orbitals, thereby effectively enhancing metal–oxygen bond stability. This orbital modulation effect originates from the synergistic electronic interactions between 3d transition metals (Fe/Co/Ni) and 4d/5d high-period metals (Mo/W); this constitutes the key mechanism for improving the catalytic activity for the oxygen reduction reaction (ORR). Density functional theory calculations reveal substantially reduced activation energy barriers for critical ORR steps in this multimetallic alloy: the energy barriers for the first step ($O_2 \rightarrow$ HOO) and third step (O → *HO) are merely 0.11 eV and 0 eV, respectively. These values demonstrate superior kinetic characteristics compared to FeCoNi (0.45 eV, 0.20 eV) and FeCoNiMo (0.30 eV, 0.06 eV) systems. The theoretical predictions align well with experimental observations, including the enhanced half-wave potential ($\Delta E_{1/2}$ = +78 mV) and near-ideal electron transfer number, confirming the optimized reaction pathway through the multimetallic synergy.

In another study, Jin *et al.* designed and synthesized ultra-small HEA nanoclusters (~2 nm) loaded on HEO nanowires for Zn–air batteries.[161] Notably, both HEA nanoclusters and HEO nanowires can be tuned separately. This type of HEA@HEO catalyst is bifunctional, demonstrating excellent performance in both the ORR and OER. The HEO is highly active for the OER, while the HEA clusters are responsible for high ORR activity, resulting in a record-low $\Delta E$ of 0.61 V. Compared with Pt@HEO, HEA@HEO exhibited improved ORR activity with significantly less Pt usage, reducing synthesis costs and making it more feasible for large-scale applications.[161] This HEA system demonstrates a remarkable


This journal is © the Partner Organisations 2025

Published on 06 May 2025. Downloaded on 8/5/2025 11:23:10 AM.



**Table 3** Summary of HEM-based catalyst for OER

| Materials | Synthesis method | Morphology | Size | Tafel slope | Electrolyte | Overpotential | Ref. |
|---|---|---|---|---|---|---|---|
| FeCoNiMo HEA/C | High temperature reduction | Particle | 8 ± 0.3 nm | N.A. | 1 M KOH | 250 mV | 148 |
| CoCrFeNiMo | Powder metallurgy | Porous | N.A. | 59.0 mV $dec^{-1}$ | 1 M KOH | 220 mV | 149 |
| FeCoNiCuPd film/CFC | Magnetron sputtering | Film on carbon fiber cloth | 2 mm | 39.8 mV $dec^{-1}$ | 1 M KOH | 194 mV | 74 |
| $(CrFeCoNi)_{97}O_3$ bulk O-HEA | Metallurgy | Bulk | N.A. | 29 mV $dec^{-1}$, | 1 M KOH | 196 mV | 72 |
| $La_{0.6}Sr_{0.4}Co_{0.2}Fe_{0.2}Mn_{0.2}Ni_{0.2}Mg_{0.2}O_3$ | Sol–gel | Particle | 40 nm | 45 mV $dec^{-1}$, | 1 M KOH | 320 mV | 83 |
| FeCoNiMnPd | Synergistic confinement | Particle | 150 nm | 96 mV $dec^{-1}$ | 1 M KOH | 390 mV | 150 |
| FeCoMoPB | Chemical reduction | Amorphous nanoplate | 20 nm | 38 mV $dec^{-1}$ | 1 M KOH | 239 mV | 153 |
| FeCoNiCrMo | Powder metallurgy | Porous | N.A. | 38.5 mV $dec^{-1}$ | 1 M KOH | 303 mV (100 mA $cm^{-2}$) | 154 |
| HE–MOFs | MOF | Nanosheet | N.A. | 59 mV $dec^{-1}$ | 1 M KOH | 274 mV | 155 |
| FeCoNiPB | Chemical reduction | | N.A. | 53 mV $dec^{-1}$ | 1 M KOH | 235 mV | 151 |
| np-UHEA12 | One-step dealloying | Nanoporous ultra-HEA ribbons | 30–40 mm thick | 84.2 mV $dec^{-1}$ | 1 M KOH | 258 mV | 134 |
| CoNiCuMnAl@C | Precipitation and pyrolysis | Spherical nano-particles | N.A. | 35.6 mV $dec^{-1}$ | 1 M KOH | 215 mV | 82 |
| ZnFeNiCuCoRu-O HEOs | Ion exchange | Hollow skeleton structure | ≈200–250 nm | 56 mV $dec^{-1}$ | 1 M KOH | 170 mV | 84 |
| $La_{0.6}Sr_{0.4}Co_{0.2}Fe_{0.2}Mn_{0.2}Ni_{0.2}Mg_{0.2}O_3$ | Sol–gel | Near-spherical | ≈70–100 nm | 45 mV $dec^{-1}$ | 1 M KOH | 320 mV | 83 |
| $(Cr_{0.2}Mn_{0.2}Fe_{0.2}Co_{0.2}Ni_{0.2})_3O_4$ NFs | Electrospinning and calcination | Oxide nanofibers | Over 10 nm | 41 mV $dec^{-1}$ | 1 M KOH | 360 mV | 156 |
| CoFeNiMoWTe NHECGs | Hierarchical hybrid | Nanosheet arrays | ≈10 nm thickness | 66.8 mV $dec^{-1}$ | 0.5 M $H_2SO_4$ | 373 mV | 157 |
| NiFeCoMnAl oxide | Electrodeposition and dealloying | Nanoporous | N.A. | 47.62 mV $dec^{-1}$ | 1 M KOH | 190 mV | 158 |
| FeCoNiMoAl | As-cast melt-extracted and cooling | Core–shell | N.A. | 39.8 mV $dec^{-1}$ | 1 M KOH | 223 mV | 159 |
| $NiFeXO_4$ | Eutectic dealloying | Nanowires | Diameter 200 nm and 10 μm long | 53.3 mV $dec^{-1}$ | 1 M KOH | 195 mV | 160 |
| PtPdAuAgCuIrRu | Alloying–dealloying | Nanoclusters | 1.5–2 nm | 49.3 mV $dec^{-1}$ | 1 M KOH | 240 mV | 161 |
| FeCoNiCrMo | Arc melting | Plate | 0.5 × 10 × 14 mm | 38.5 mV $dec^{-1}$ | 1 M KOH | 303 mV (100 mA $cm^{-2}$) | 154 |
| $Ni_{14}Co_{14}Fe_{14}Mo_6Mn_{52}$ | Single-roller melt spinning | Nanoporous | 200–300 nm diameter | 37 mV $dec^{-1}$ | 1 M KOH | 243 mV | 71 |
| AlCrCuFeNi | Vacuum induction melting | Nanoporous particles | N.A. | 77.5 mV $dec^{-1}$ | 1 M KOH | 270 mV | 162 |
| FeCoNiCuMn/CNFs | Polymer fiber nanoreactor | 3D network nanofibers | 12.9 ± 6.6 nm | 69 mV $dec^{-1}$ | 1 M KOH | 386 mV (200 mA $cm^{-2}$) | 163 |
| FeCoNiMnRu | Electrospinning and graphitization | Nanoporous particles | 14.2 ± 9.1 nm | 67.4 mV $dec^{-1}$ | 1 M KOH | 308 mV (100 mA $cm^{-2}$) | 139 |
| $(CrFeCoNiMo)_3O_4$ | N.A. | Nanosheets | N.A. | 37.0 mV $dec^{-1}$ | 1 M KOH | 255.3 mV | 164 |
| $(FeCoNiCrMn)_3O_4$ | Electrospinning | N.A. | N.A. | 71.38 mV $dec^{-1}$ | 1 M KOH | 318.4 mV | 165 |
| $(CrMnFeCoNi)_3O_4$ | Electrospun | Fiber | N.A. | 41 mV $dec^{-1}$ | 1 M KOH | 360 mV | 156 |
| (FeCoNiCuZn)O | Sol–gel | Particle | 200 nm–1 mm | 64.5 mV $dec^{-1}$ | 1 M KOH | 323 mV | 33 |
| $(Fe_{0.2}Co_{0.2}Ni_{0.2}Cr_{0.2}Mn_{0.2})_3O_4$ | Solution combustion | Porous | 10 nm | 50.27 mV $dec^{-1}$ | 1 M KOH | 275 mV | 166 |

This journal is © the Partner Organisations 2025

Published on 06 May 2025. Downloaded on 8/5/2025 11:23:10 AM.

activity enhancement mechanism. The precise regulation of oxygen adsorption energy ($\Delta E_O$) constitutes the core factor. $\Delta E_O$ on HEA surfaces is 0.2 eV lower than that of Pt (111), with a deviation of less than 0.01 eV from the theoretical optimal adsorption energy (0.2 eV weaker than Pt). This near-ideal adsorption strength significantly accelerates the ORR kinetics. This characteristic originates from the synergistic electronic effects of multiple metallic components (Pt, Pd, Au, Ag, Ir, Ru), which reconstruct the surface electronic structure to effectively reduce oxygen adsorption barriers. Furthermore, electronic structure analysis reveals that the d-band center of Pt in HEA shifts downward to −1.818 eV, showing a notable negative displacement compared to pure Pt (111) (−1.789 eV). This multimetallic interface-induced d-band center downshift weakens the O–Pt bonding strength, accelerates the desorption kinetics of ORR intermediates, and ultimately achieves a comprehensive improvement in catalytic efficiency.

As shown in Fig. 14a, Huang *et al.* proposed a simple microenvironment regulation strategy to modulate solvent polarity and nanoparticle–support interactions within precursors for carbon thermal shock pyrolysis.[174] They found that reducing solvent polarity and enhancing particle–support affinity could jointly control the nanoparticle size, ultimately achieving a size of approximately 2.68 nm with a Pt loading of ~10 wt%. This approach improves the catalytic performance and reduces the preparation cost of the catalyst. Additionally, Zou *et al.* synthesized self-supporting HEA-O (oxygen-doped high-entropy alloys) using a rapid Joule heating method.[175] As demonstrated in Fig. 14b, the O-doped HEAs (HEA-O) exhibited exceptional performance and stability in water electrolysis and zinc–air batteries, remaining stable for over 1600 h and capable of reassembly after zinc consumption.

Qiu *et al.* proposed a novel dual-active center alloying strategy to achieve efficient bifunctional oxygen catalysis and further employed the high-entropy effect to regulate the structure and performance of the catalyst,[179] as shown in the schematic in Fig. 14c. Notably, the resulting HEA catalyst demonstrates outstanding catalytic activity for both the OER and ORR, with a peak power density of 136.53 mW $cm^{-2}$ and an energy density of 987.9 mA h $g_{Zn}^{-1}$, surpassing most previously reported bifunctional oxygen electrocatalysts. Furthermore, the assembled flexible rechargeable zinc–air battery (ZAB) shows an excellent performance even at an ultralow temperature of −40 °C (Fig. 14d).

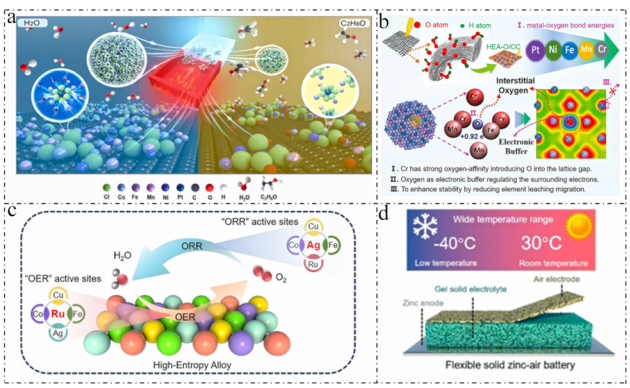


**Fig. 14** (a) PtFeCoNiMn high-entropy alloy supported on carbon *via* the CTS method (cited from ref. 176). (b) Schematic illustration of the synthesis process and mechanism of HEA-O (cited from ref. 177). (c) Schematic of the design of the dual-active-center HEA catalyst. (d) Schematic diagram of wide-temperature FSZABs (cited from ref. 178).

As summarized in Table 4, we provide a comparison and analysis of other recent high-entropy catalysts for the ORR alongside those already described.

### 5.4 Overall water splitting

Overall water splitting, a promising route to sustainable hydrogen production, faces three critical challenges that hinder its practical implementation.[194] First, conventional catalysts struggle to achieve dual-functionality by simultaneously optimizing HER and OER activities, as the electronic and geometric requirements for these two processes often conflict. Second, the high overpotential driven by sluggish OER kinetics, particularly at the anode, significantly elevates energy consumption. Third, stability degradation caused by catalyst dissolution or structural collapse under harsh acidic/alkaline operating conditions limits long-term durability. To address these challenges, HEMs emerge as a revolutionary platform owing to their unique structural and electronic properties. The multi-element synergy in HEMs, exemplified by tailored compositions such as Ni–Fe–Co–Mn–Cr systems, enables the coexistence of dual-active sites that balance adsorption energies for HER/OER intermediates (*e.g.*, H and OOH species), thereby optimizing bifunctional activity. Furthermore, the inherent structural resilience of HEMs, arising from high-entropy effects, mitigates elemental segregation and phase transformations under dynamic electrochemical conditions, ensuring prolonged stability. Notably, bifunctional design strategies, such as constructing heterostructured interfaces between high-entropy alloys (HEAs) and oxides (HEOs), spatially decouple HER and OER active regions while minimizing interfacial charge transfer resistance. For instance, HEA/HEO heterojunctions leverage the metallic conductivity of HEAs for efficient electron transport during the HER and the oxide-rich surfaces of HEOs for stabilizing OER intermediates, achieving synergistic performance enhancement. These advancements position HEMs as a transformative solution to overcome the limitations of traditional catalysts in overall water splitting systems.

Cha *et al.* employed a xenon lamp flash-induced photothermal shock method to rapidly synthesize multielement HEA-NPs on CNF supports.[195] By subjecting the CNF surface to instantaneous heating followed by ultrafast cooling, PtIrFeNiCoCe hexanary solid-solution NPs were synthesized, effectively suppressing phase separation governed by conventional thermodynamics. The millisecond-level non-equilibrium process enabled large-area uniform coating (6 × 6 $cm^2$), circumventing alloying theory limitations. Synergy between high-entropy effects and ultrafast kinetics facilitated atomic-scale homogenization: Pt/Ir provided efficient HER active sites, Fe/Ni/Co optimized *OOH intermediate adsorption for the


This journal is © the Partner Organisations 2025

Published on 06 May 2025. Downloaded on 8/5/2025 11:23:10 AM.

Table 4 Summary of HEM-based catalyst for ORR

| Materials | Synthesis method | Morphology | Size | Halfwave potential | Test conditions | Ref. |
|---|---|---|---|---|---|---|
| FeCoNiCuPd OHEA-mNC | *In situ* construct | 2D mesoporous | 10 nm | 0.9 V | Alkaline | 180 |
| $Pt(FeCoNiCuZn)_3/C$ | Impregnation–reduction | Nanoparticle | 12 nm | 0.80 V | Acidic | 181 |
| NMnFeCoNiCu HESA | Wet chemical | Single atom | N.A. | 0.87 V | Alkaline | 176 |
| $Pt_4FeCoCuNi$ | Sulfur-anchoring | Particle | 5.1 nm | 0.943 V | Acidic | 137 |
| AlCoFeMoCr/Pt | Top-down | Particle | 1–2 nm | 0.88 V | Alkaline | 177 |
| PtIrFeCoCu | Chemically reduced | Particle | 6 nm | 0.894 V | Acidic | 178 |
| CrMnFeCoNi | Solvothermal | Particle | 170 nm | 0.78 V | Alkaline | 182 |
| FeCoNiMoW | Solvothermal | Particle | 35 ± 20 nm | 0.71 V | Alkaline | 173 |
| HEA-NPs-(14) | Alloying | Particle | 5 nm | 0.86 V | Alkaline | 183 |
| FeCoNiCuMn | Movable printing | N.A. | N.A. | 0.887 V | Alkaline | 184 |
| Pt4FeCoCuNi | Impregnation method | Nanoparticle | 5 nm | 0.943 V | Alkaline | 137 |
| PtPdAuAgCuIrRu | Alloying–dealloying | Nanoclusters | 1.5–2 nm | 0.89 V | Alkaline | 161 |
| AlNiCoRuMo | Alloying–dealloying | Nanowire | ~20–100 nm | 0.875 V | Alkaline | 185 |
| 6-HENs/PC | Anchoring–carbonization | Nanoparticle | 2.2 nm | 0.898 V | Alkaline | 186 |
| 10-HEO/C | Far-equilibrium synthesis | Nanoparticle | ~7 nm | 0.85 V | Alkaline | 28 |
| $FeCoNiO_x$@IrPt | One-step synthesis | Nanoparticles | ~5 nm | 0.83 V | Alkaline | 187 |
| PtPdRhRuIrFeCoNi MMNCs | Thermal shock | Nanoparticles | N.A. | 0.85 V | Alkaline | 188 |
| FeCoNiMoW | Colloidal-based approach | Nanoparticles | 35 ± 20 nm | 0.71 V | Alkaline | 173 |
| PtPdFeCoNi | High-temperature injection | Nanoparticles | 12 ± 4 nm | 0.92 V | Alkaline | 82 |
| HEA@Pt | *In situ* growth | Nanoparticles | 23 nm | 0.85 V | Alkaline | 189 |
| FeCoNiMnCrO | Electric dipole transition | Nanoparticles | N.A. | 0.87 V | Alkaline | 190 |
| Li-HEO | Ball milling | Particle | 2 μm | N.A. | N.A. | 191 |
| $(Pr_{0.25}La_{0.25}Nd_{0.25}Ca_{0.25})_2NiO_{4+\delta}$ | Sol–gel | Particle | N.A. | N.A. | N.A. | 192 |
| Ru@HEPO | Sol–gel | Particle | 100 nm | N.A. | N.A. | 193 |

OER, and Ce acted as an electronic modulator to inhibit metal dissolution. The CNF support enhanced electron transfer and mass diffusion through its high conductivity and photothermal-induced surface defects, while maximizing active site exposure. A symmetric electrolyzer achieved overall water splitting in 0.1 M KOH with a total overpotential of 777 mV@10 mA $cm^{-2}$, surpassing most reported HEA catalysts. Long-term stability tests revealed >95% performance retention after 5000 cycles at 10 mA $cm^{-2}$, with SEM/EDS confirming negligible NP aggregation or elemental leaching and hypochlorite byproduct concentration of <0.03 ppm. Theoretically, this work demonstrates that the interplay between ultrafast heating/cooling and high entropy is pivotal for phase-separation suppression and atomic-level mixing, establishing a novel paradigm for designing efficient and stable nano-catalytic systems.

### 5.5 Seawater splitting

Seawater splitting, an economically attractive alternative to freshwater-based electrolysis, faces three critical barriers that impede its industrial scalability. First, chloride-induced corrosion triggered by the competing ClER at high anodic potentials not only reduces faradaic efficiency for oxygen evolution but also accelerates catalyst degradation through pitting and oxidative etching. Second, impurity poisoning caused by the deposition of $Mg^{2+}$ and $Ca^{2+}$ ions—abundant in seawater—physically blocks active sites and disrupts ion transport pathways. Third, the slow reaction kinetics under high-salinity conditions stems from altered electrolyte conductivity, ion hydration structures, and intermediate adsorption/desorption energetics. To overcome these challenges, HEMs offer a multifaceted solution, leveraging their intrinsic chemical complexity. The corrosion resistance of HEMs arises from self-passivating surfaces enriched with corrosion-resistant elements (*e.g.*, Cr/Mo-rich oxides), which form dense, chemically inert layers that inhibit $Cl^-$ penetration while maintaining catalytic activity. Simultaneously, selectivity engineering *via* electronic structure modulation—such as tuning the d-band center of transition metal sites—weakens Cl adsorption affinity (*e.g.*, reducing $Cl^- \rightarrow Cl$ binding energy) while enhancing $H_2O$ dissociation kinetics, thereby suppressing ClER and promoting the selective OER. For instance, Mo-doped HEMs exhibit a 30% reduction in ClER current density compared to conventional catalysts (performance data to be supplemented). Furthermore, the self-cleaning capability of HEMs, enabled by dynamic elemental redistribution under operational conditions, continuously refreshes active surfaces by dissolving or redistributing deposited impurities (*e.g.*, Mg/Ca species), as evidenced by *in situ* atomic force microscopy studies. These synergistic properties position HEMs as a robust and adaptive catalyst platform for seawater electrolysis, addressing both thermodynamic and kinetic limitations inherent to marine environments. Feng *et al.* synthesized an $(FeCoNiMnAl)_3O_4$/NF electrode with a 3D hierarchical microflower architecture by hydrothermally growing FeCoNiMnAl hydroxide precursors on nickel foam (NF), followed by annealing.[196] In this material, the incorporation of Al effectively reduced the oxygen evolution reaction (OER) energy barrier, while Mn exhibited a synergistic effect to enhance the intrinsic activity. The microflower structure, composed of densely stacked nanosheets, offered a high specific surface area and abundant active sites. During seawater electrolysis, the electrode demonstrated outstanding performance, requiring overpotentials of only 284 mV and 295 mV to achieve a current density of 50 mA $cm^{-2}$ in alkaline

Published on 06 May 2025. Downloaded on 8/5/2025 11:23:10 AM.

simulated seawater (1 M KOH + 0.5 M NaCl) and natural seawater electrolytes, respectively. Remarkably, it maintained a stable OER activity for 50 h at 500 mA $cm^{-2}$ without significant corrosion or structural degradation. DFT calculations revealed that the Ni sites exhibited a high charge carrier density in their d-orbitals near the Fermi level, facilitating interfacial charge transfer and optimizing the adsorption free energy of *OOH intermediates, thereby accelerating the OER kinetics.

Park *et al.* synthesized AuRuIrPdPt high-entropy alloys (HEAs) with floral and hairy spherical morphologies by irradiating metal salt solutions for 90 s using a continuous-wave $CO_2$ laser at 30%, 60%, and 90% of 25 W power.[197] Raman spectroscopy revealed the emergence of Pt–O, Pd–O, and Ru–H bond signatures under applied potential, indicating that Pt and Pd facilitated water dissociation, while Ru served as the primary active site for H* adsorption/desorption. The synergistic interplay between Ru, Pd, and Pt significantly reduced the energy barrier for the HER Volmer step. The optimized HEA-60 catalyst exhibited exceptional HER activity with overpotentials of 37 mV, 34 mV, and 45 mV at 10 mA $cm^{-2}$ in alkaline, simulated seawater (1 M KOH + 0.5 M NaCl), and natural seawater electrolytes, respectively, surpassing commercial Pt/C (52 mV@alkaline). An overall water-splitting (OWS) electrolyzer assembled with HEA-60 as the cathode and $IrO_2$ as the anode achieved a cell voltage of only 1.62 V at 10 mA $cm^{-2}$ in natural seawater, maintaining 80% faradaic efficiency after 60 min of operation. The electrolyzer demonstrated remarkable durability with negligible voltage decay and minimal hypochlorite byproduct generation (<0.05 ppm), highlighting its corrosion-resistant design. Besides, Xie *et al.* synthesized FeNiCoCrRu high-entropy alloy nanoparticles (HEA NPs) *in situ* on carbon paper *via* $CO_2$ laser-induced rapid conversion of metal precursors,[198] forming a single-phase solid-solution structure with pronounced lattice distortion and electron transfer, which collectively enhanced the catalytic performance. In alkaline seawater electrolyte (1 M KOH + 0.5 M NaCl), the material exhibited exceptional bifunctional activity, requiring overpotentials of only 52 mV for the hydrogen evolution reaction (HER) and 320 mV for the oxygen evolution reaction (OER) at 100 mA $cm^{-2}$. The assembled FeNiCoCrRu||FeNiCoCrRu electrolyzer achieved overall seawater splitting voltages of 1.594 V, 1.683 V, and 1.808 V at current densities of 10, 50, and 100 mA $cm^{-2}$, respectively, outperforming the conventional Pt/C||$RuO_2$ system (1.746 V@100 mA $cm^{-2}$). Notably, faradaic efficiencies reached 99.6% for $H_2$ and 97.7% for $O_2$. The electrolyzer demonstrated remarkable durability, with a minimal voltage increase of 0.153 V after 3050 h of continuous operation at 250 mA $cm^{-2}$, accompanied by negligible hypochlorite generation (<0.1 ppm) and metal dissolution (<0.5 μg $L^{-1}$), highlighting its superior corrosion resistance. Electronic structure analysis revealed a downward shift of the Ru 3p binding energy, indicative of electron transfer from 3d transition metals (Fe, Co, Ni, Cr) to Ru atoms, which optimized the adsorption free energy of hydrogen/oxygen intermediates and accelerated the reaction kinetics. Furthermore, the electrolyzer maintained its stable operation at 100 mA $cm^{-2}$ under varying electrolyte concentrations and temperatures, underscoring its broad applicability.

# 6 Summary and prospects

High-entropy materials (HEMs), characterized by their multielement composition, diverse active sites, and high-entropy-stabilized structures, demonstrate exceptional performance in electrocatalysis.[199,200] These distinctive features not only enhance the catalytic efficiency but also confer remarkable stability under operational conditions. As a result, HEMs present significant potential for further development in a wide range of applications.

To fully realize the potential of HEMs in electrocatalysis and other fields, integrating research on these materials with emerging technologies presents both challenges and opportunities. By capitalizing on advancements in artificial intelligence, advanced characterization methods, nanotechnology, additive manufacturing, and sustainable practices, the innovation and performance of high-entropy catalysts can be significantly accelerated. The following perspectives outline proposed strategies for advancing the development of HEMs in catalysis, offering guidance and direction for future research and development endeavors.

## 6.1 Mechanism of high-entropy catalysts

The catalytic performance of HEMs is governed by complex interactions among the constituent elements, which give rise to their unique properties. However, the exact mechanisms behind their enhanced catalytic activity remain unclear. The lattice distortion caused by the multi-element composition is thought to modify the electronic structure, potentially shifting the D-band center, which influences the adsorption of reactants and thus the overall catalytic efficiency. To deepen our understanding of these mechanisms, future research must combine advanced theoretical simulations, such as density functional theory (DFT), with cutting-edge characterization methods to more accurately probe the dynamic evolution of active sites in HEMs.

## 6.2 Component regulation and synthesis strategy

Additionally, the size, shape, and morphology of synthesized HEMs strongly influence the number and accessibility of active sites, thereby affecting the catalytic performance. Current methods for synthesizing various forms of HEMs are still limited, and new processing routes are essential for scaling up their production to meet growing demand. Furthermore, when dealing with high-entropy substrates, factors such as substrate adhesion, coating layers, and the design of interfaces can significantly affect performance and stability. Achieving a balance between form and function, while ensuring long-term stability under harsh operational conditions, remains a critical challenge for HEMs in electrocatalysis. As such, future research should explore new strategies for component regulation,


This journal is © the Partner Organisations 2025

Published on 06 May 2025. Downloaded on 8/5/2025 11:23:10 AM.

including the introduction of interface effects and the optimization of local stress–strain distributions, which could further enhance the catalytic activity. Besides, to go beyond Sabatier's prediction and further improve the catalytic performance of the material, other variables such as interface effects and local stress–strain design need to be introduced.

Afterall, utilize computational simulations, such as DFT, to pre-screen and identify optimal combinations of reactants in order to forecast their behavior in specific reactions. According to experimental data, the composition ratio is constantly adjusted to find the optimal performance combination. This task is complicated by the vast compositional space available for HEMs, making it difficult to predict which combinations will perform best. To address this challenge, integrating computational tools, such as machine learning and simulation-based screening methods, can significantly enhance the efficiency of material selection. In particular, DFT and other simulation techniques can be used to pre-screen compositions and predict the behavior of different material combinations in specific catalytic reactions.

### 6.3 Prospects for applications and development

The nearly unlimited compositional space available for HEMs offers immense potential for synthesizing electrochemical catalysts. Recently, there has been a trend towards using low-cost transition metals to create high-entropy catalysts that reduce or even replace precious metals traditionally used in catalytic materials. Non-noble metal high-entropy catalysts have demonstrated catalytic performances close to or surpassing commercial Pt/C ruthenium oxide; however, complexities in preparation processes and stability under harsh conditions (*e.g.*, acidic environments) remain issues. Future research must focus on maintaining an excellent performance while improving stability and simplifying the preparation process for non-precious metal catalysts.

In addition to their potential as standalone electrocatalysts, HEMs can be integrated with emerging technologies, such as nanotechnology, artificial intelligence, and advanced manufacturing techniques, to further enhance their performance and broaden their application scope. The synergy between these complementary fields presents both challenges and exciting opportunities. By leveraging advancements in these areas, it is possible to accelerate the development and application of high-entropy catalysts in various sectors, including energy conversion and storage.

### 6.4 Environmental impact and sustainability

HEMs, particularly those designed to reduce or eliminate the use of precious metals, offer significant environmental advantages by addressing key ecological challenges associated with traditional catalytic materials. These catalysts, characterized by their multielement compositions and high configurational entropy, not only provide enhanced catalytic activity but also minimize the need for scarce and resource-intensive precious metals such as Pt, Pd, and Au. The extraction and processing of these precious metals are environmentally disruptive, contributing to habitat destruction, toxic waste generation, and high energy consumption. By replacing them with more abundant, less toxic elements like Fe, Ni, and Cu, HEMs reduce the ecological pressures associated with mining and refining, while maintaining or even improving catalytic performance. Furthermore, the use of more stable and less reactive elements in HEMs extends their lifespan, reduces the frequency of catalyst replacement, and mitigates issues like poisoning or sintering, which are common with traditional catalysts. These properties enhance the sustainability of catalytic processes, aligning with circular economy principles by facilitating recycling and reuse. The environmental impact of HEMs is further reduced through more efficient recycling processes, which are made possible by the lower toxicity and greater stability of the constituent elements. As such, high-entropy catalysts represent a promising solution for reducing the ecological footprint of catalytic processes, particularly in energy conversion and storage applications. However, widespread adoption of HEMs will require continued advancements in the synthesis, scalability, and recycling of these materials, driven by interdisciplinary collaboration between materials science, green chemistry, and environmental engineering. Through such efforts, HEMs have the potential to play a pivotal role in shaping a more sustainable future for catalysis and energy technologies.

Despite some challenges remaining unresolved, it is undeniable that the research space and application prospects for HEMs are burgeoning. Collective efforts from scientific researchers worldwide have propelled rapid advancements in this field, paving the way for large-scale applications across diverse domains. As investigations continue to unravel the multifaceted properties and functionalities of HEMs, their significance in energy fields becomes increasingly apparent.

In conclusion, the interdisciplinary approach for HEM research, integrating theoretical modeling, experimental innovation, and technological advancements, will likely propel HEMs into a leading position in the field of electrocatalysis. With ongoing research, HEMs hold the potential to significantly advance energy conversion technologies, reduce the reliance on precious metals, and contribute to a more sustainable future in catalysis. The continued exploration of these materials promises to unlock new functionalities and improve the efficiency of various catalytic processes, making them indispensable in addressing global energy challenges.

## Data availability

No primary research results, software or code have been included and no new data were generated or analysed as part of this review.

## Conflicts of interest

There are no conflicts to declare.

Published on 06 May 2025. Downloaded on 8/5/2025 11:23:10 AM.

## References


1 Y. Sun and S. Dai, High-entropy materials for catalysis: A new frontier, *Sci. Adv.*, 2021, **7**, eabg1600.
2 A. Amiri and R. Shahbazian-Yassar, Recent progress of high-entropy materials for energy storage and conversion, *J. Mater. Chem. A*, 2021, **9**, 782–823.
3 X. Li, Y. Zhou, C. Feng, R. Wei, X. Hao, K. Tang and G. Guan, High entropy materials based electrocatalysts for water splitting: Synthesis strategies, catalytic mechanisms, and prospects, *Nano Res.*, 2023, **16**, 4411–4437.
4 E. P. George, D. Raabe and R. O. Ritchie, High-entropy alloys, *Nat. Rev. Mater.*, 2019, **4**, 515–534.
5 J.-T. Ren, L. Chen, H.-Y. Wang and Z.-Y. Yuan, High-entropy alloys in electrocatalysis: from fundamentals to applications, *Chem. Soc. Rev.*, 2023, **52**, 8319–8373.
6 X. Chang, M. Zeng, K. Liu and L. Fu, Phase Engineering of High–Entropy Alloys, *Adv. Mater.*, 2020, **32**, 1907226.
7 S. Akrami, P. Edalati, M. Fuji and K. Edalati, High-entropy ceramics: Review of principles, production and applications, *Mater. Sci. Eng., R*, 2021, **146**, 100644.
8 K. Wang, W. Hua, X. Huang, D. Stenzel, J. Wang, Z. Ding, Y. Cui, Q. Wang, H. Ehrenberg, B. Breitung, C. Kübel and X. Mu, Synergy of cations in high entropy oxide lithium ion battery anode, *Nat. Commun.*, 2023, **14**, 1487.
9 G. N. Kotsonis, S. S. I. Almishal, F. Marques Dos Santos Vieira, V. H. Crespi, I. Dabo, C. M. Rost and J. Maria, High–entropy oxides: Harnessing crystalline disorder for emergent functionality, *J. Am. Ceram. Soc.*, 2023, **106**, 5587–5611.
10 M. Cui, C. Yang, B. Li, Q. Dong, M. Wu, S. Hwang, H. Xie, X. Wang, G. Wang and L. Hu, High–Entropy Metal Sulfide Nanoparticles Promise High–Performance Oxygen Evolution Reaction, *Adv. Energy Mater.*, 2021, **11**, 2002887.
11 R. Mohili, N. R. Hemanth, H. Jin, K. Lee and N. Chaudhari, Emerging high entropy metal sulphides and phosphides for electrochemical water splitting, *J. Mater. Chem. A*, 2023, **11**, 10463–10472.
12 D. Wu, K. Kusada, Y. Nanba, M. Koyama, T. Yamamoto, T. Toriyama, S. Matsumura, O. Seo, I. Gueye, J. Kim, L. S. Rosantha Kumara, O. Sakata, S. Kawaguchi, Y. Kubota and H. Kitagawa, Noble-Metal High-Entropy-Alloy Nanoparticles: Atomic-Level Insight into the Electronic Structure, *J. Am. Chem. Soc.*, 2022, **144**, 3365–3369.
13 R. Guo and T. He, High-Entropy Perovskite Electrolyte for Protonic Ceramic Fuel Cells Operating below 600 °C, *ACS Mater. Lett.*, 2022, **4**, 1646–1652.
14 I. Hussain, C. Lamiel, M. Ahmad, Y. Chen, S. Shuang, M. S. Javed, Y. Yang and K. Zhang, High entropy alloys as electrode material for supercapacitors: A review, *J. Energy Storage*, 2021, **44**, 103405.
15 Y. Chen, H. Fu, Y. Huang, L. Huang, X. Zheng, Y. Dai, Y. Huang and W. Luo, Opportunities for High-Entropy Materials in Rechargeable Batteries, *ACS Mater. Lett.*, 2021, **3**, 160–170.
16 J.-W. Yeh, S.-K. Chen, S.-J. Lin, J.-Y. Gan, T.-S. Chin, T.-T. Shun, C.-H. Tsau and S.-Y. Chang, Nanostructured High-Entropy Alloys with Multiple Principal Elements: Novel Alloy Design Concepts and Outcomes, *Adv. Eng. Mater.*, 2004, **6**, 299–303.
17 B. Cantor, I. T. H. Chang, P. Knight and A. J. B. Vincent, Microstructural development in equiatomic multicomponent alloys, *Mater. Sci. Eng., A*, 2004, **375–377**, 213–218.
18 A. Peker and W. L. Johnson, A highly processable metallic glass: Zr41.2Ti13.8Cu12.5Ni10.0Be22.5, *Appl. Phys. Lett.*, 1993, **63**, 2342–2344.
19 Y. Xin, S. Li, Y. Qian, W. Zhu, H. Yuan, P. Jiang, R. Guo and L. Wang, High-Entropy Alloys as a Platform for Catalysis: Progress, Challenges, and Opportunities, *ACS Catal.*, 2020, **10**, 11280–11306.
20 L. Yu, K. Zeng, C. Li, X. Lin, H. Liu, W. Shi, H. Qiu, Y. Yuan and Y. Yao, High–entropy alloy catalysts: From bulk to nano toward highly efficient carbon and nitrogen catalysis, *Carbon Energy*, 2022, **4**, 731–761.
21 Y. Ma, Y. Ma, Q. Wang, S. Schweidler, M. Botros, T. Fu, H. Hahn, T. Brezesinski and B. Breitung, High-entropy energy materials: challenges and new opportunities, *Energy Environ. Sci.*, 2021, **14**, 2883–2905.
22 Z. Wang, J. You, Y. Zhao, R. Yao, G. Liu, J. Lu and S. Zhao, Research progress on high entropy alloys and high entropy derivatives as OER catalysts, *J. Environ. Chem. Eng.*, 2023, **11**, 109080.
23 Z. Li, K. G. Pradeep, Y. Deng, D. Raabe and C. C. Tasan, Metastable high-entropy dual-phase alloys overcome the strength–ductility trade-off, *Nature*, 2016, **534**, 227–230.
24 B. Gludovatz, A. Hohenwarter, D. Catoor, E. H. Chang, E. P. George and R. O. Ritchie, A fracture-resistant high-entropy alloy for cryogenic applications, *Science*, 2014, **345**, 1153–1158.
25 S. Qin, M. Yang, P. Jiang, J. Wang, X. Wu, H. Zhou and F. Yuan, Designing structures with combined gradients of grain size and precipitation in high entropy alloys for simultaneous improvement of strength and ductility, *Acta Mater.*, 2022, **230**, 117847.
26 J. Kwon, S. Sun, S. Choi, K. Lee, S. Jo, K. Park, Y. K. Kim, H. B. Park, H. Y. Park, J. H. Jang, H. Han, U. Paik and T. Song, Tailored Electronic Structure of Ir in High Entropy Alloy for Highly Active and Durable Bifunctional Electrocatalyst for Water Splitting under an Acidic Environment, *Adv. Mater.*, 2023, **35**, 2300091.
27 C. R. McCormick and R. E. Schaak, Simultaneous Multication Exchange Pathway to High-Entropy Metal Sulfide Nanoparticles, *J. Am. Chem. Soc.*, 2021, **143**, 1017–1023.
28 T. Li, Y. Yao, B. H. Ko, Z. Huang, Q. Dong, J. Gao, W. Chen, J. Li, S. Li, X. Wang, R. Shahbazian-Yassar, F. Jiao and L. Hu, Carbon-Supported High-Entropy Oxide Nanoparticles as Stable Electrocatalysts for Oxygen Reduction Reactions, *Adv. Funct. Mater.*, 2021, **31**, 2010561.
29 D. Lai, Q. Kang, F. Gao and Q. Lu, High-entropy effect of a metal phosphide on enhanced overall water splitting performance, *J. Mater. Chem. A*, 2021, **9**, 17913–17922.


 This journal is © the Partner Organisations 2025

Published on 06 May 2025. Downloaded on 8/5/2025 11:23:10 AM.

30 R. Tu, K. Liang, Y. Sun, Y. Wu, W. Lv, C. Q. Jia, E. Jiang, Y. Wu, X. Fan, B. Zhang, Q. Lu, B. Zhang and X. Xu, Ultra-Dilute high-entropy alloy catalyst with core-shell structure for high-active hydrogenation of furfural to furfuryl alcohol at mild temperature, *Chem. Eng. J.*, 2023, **452**, 139526.
31 D. Feng, Y. Dong, P. Nie, L. Zhang and Z.-A. Qiao, CoNiCuMgZn high entropy alloy nanoparticles embedded onto graphene sheets via anchoring and alloying strategy as efficient electrocatalysts for hydrogen evolution reaction, *Chem. Eng. J.*, 2022, **430**, 132883.
32 X. Lincheng, W. Yue, Y. Yong, H. Zhanzhong, C. Xin and L. Fan, Triggering efficient Mn active centers by tuning the localized Sr2 + sites in high-entropy ABO3 oxygen electrocatalysis, *Chem. Eng. J.*, 2024, **485**, 149755.
33 Y. Lao, X. Huang, L. Liu, X. Mo, J. Huang, Y. Qin, Q. Mo, X. Hui, Z. Yang and W. Jiang, Structure-activity relationship study of high entropy oxides catalysts for oxygen evolution reaction, *Chem. Eng. J.*, 2024, **481**, 148428.
34 H. Nan, S. Lv, Z. Xu, Y. Feng, Y. Zhou, M. Liu, T. Wang, X. Liu, X. Hu and H. Tian, Inducing the cocktail effect in yolk-shell high-entropy perovskite oxides using an electronic structural design for improved electrochemical applications, *Chem. Eng. J.*, 2023, **452**, 139501.
35 Z. Wang, High-entropy phosphate/C hybrid nanosheets for efficient acidic hydrogen evolution reaction, *Chem. Eng. J.*, 2022, **437**, 135375.
36 S. Liao, Engineering High-Entropy Duel-Functional nanocatalysts with regulative oxygen vacancies for efficient overall water splitting, *Chem. Eng. J.*, 2023, **471**, 144506.
37 H. Li, H. Huang, Y. Chen, F. Lai, H. Fu, L. Zhang, N. Zhang, S. Bai and T. Liu, High–Entropy Alloy Aerogels: A New Platform for Carbon Dioxide Reduction, *Adv. Mater.*, 2023, **35**, 2209242.
38 S. Nellaiappan, N. K. Katiyar, R. Kumar, A. Parui, K. D. Malviya, K. G. Pradeep, A. K. Singh, S. Sharma, C. S. Tiwary and K. Biswas, High-Entropy Alloys as Catalysts for the $CO_2$ and CO Reduction Reactions: Experimental Realization, *ACS Catal.*, 2020, **10**, 3658–3663.
39 N. Kumar Katiyar, K. Biswas, J.-W. Yeh, S. Sharma and C. Sekhar Tiwary, A perspective on the catalysis using the high entropy alloys, *Nano Energy*, 2021, **88**, 106261.
40 T. Lçffler, A. Ludwig, J. Rossmeisl and W. Schuhmann, What Makes High-Entropy Alloys Exceptional Electrocatalysts ?, *Angew. Chem., Int. Ed.*, 2021, **60**, 26894–26903.
41 S. S. Aamlid, M. Oudah, J. Rottler and A. M. Hallas, Understanding the Role of Entropy in High Entropy Oxides, *J. Am. Chem. Soc.*, 2023, **145**, 5991–6006.
42 Y.-C. Qin, F.-Q. Wang, X.-M. Wang, M.-W. Wang, W.-L. Zhang, W.-K. An, X.-P. Wang, Y.-L. Ren, X. Zheng, D.-C. Lv and A. Ahmad, Noble metal-based high-entropy alloys as advanced electrocatalysts for energy conversion, *Rare Met.*, 2021, **40**, 2354–2368.
43 W. Xiao, Y. Li, A. Elgendy, E. C. Duran, M. A. Buckingham, B. F. Spencer, B. Han, F. Alam, X. Zhong, S. H. Cartmell, R. J. Cernik, A. S. Eggeman, R. A. W. Dryfe and D. J. Lewis, Synthesis of High Entropy and Entropy-Stabilized Metal Sulfides and Their Evaluation as Hydrogen Evolution Electrocatalysts, *Chem. Mater.*, 2023, **35**, 7904–7914.
44 L. Lin, K. Wang, A. Sarkar, C. Njel, G. Karkera, Q. Wang, R. Azmi, M. Fichtner, H. Hahn, S. Schweidler and B. Breitung, High–Entropy Sulfides as Electrode Materials for Li–Ion Batteries, *Adv. Energy Mater.*, 2022, **12**, 2103090.
45 Z. Yang, X. Xiang, J. Yang and Z.-Y. Zhao, High-entropy oxides as energy materials: from complexity to rational design, *Mater. Futures*, 2024, **3**, 042103.
46 W. Bao, H. Shen, Y. Zhang, C. Qian, G. Zeng, K. Jing, D. Cui, J. Xia, H. Liu, C. Guo, F. Yu, K. Sun and J. Li, High-entropy oxides for energy storage and conversion, *J. Mater. Chem. A*, 2024, **12**, 23179–23201.
47 L. Song, C. Ma, P. Shi, X. Zhu, K. Qu, L. Zhu, Q. Lu and A.-L. Wang, Self-supported FeCoNiCuP high-entropy alloy nanosheet arrays for efficient glycerol oxidation and hydrogen evolution in seawater electrolytes, *ACS Symp. Ser.*, 2024, **26**, 10921–10928.
48 Z. Yu, D. W. Boukhvalov, H. Tan, D. Xiong, C. Feng, J. Wang, W. Wang, Y. Zhao, K. Xu, W. Su, X. Xiang, F. Lin, H. Huang, F. Zhang, L. Zhang, L. Meng and L. Liu, Sulfur and phosphorus co-doped FeCoNiCrMn high-entropy alloys as efficient sulfion oxidation reaction catalysts enabling self-powered asymmetric seawater electrolysis, *Chem. Eng. J.*, 2024, **494**, 153094.
49 H. Mao, X. Qu, H. Ma, J. Chi, Z. Xiao, Y. Chai, Z. Wu, X. Liu and L. Wang, The regulation of multiple 3d orbits triggers the self-equilibrium effect of high-entropy oxide in seawater electrolysis, *J. Colloid Interface Sci.*, 2025, **688**, 611–620.
50 E. P. George, W. A. Curtin and C. C. Tasan, High entropy alloys: A focused review of mechanical properties and deformation mechanisms, *Acta Mater.*, 2020, **188**, 435–474.
51 X. Yan, Functional properties and promising applications of high entropy alloys, *Scr. Mater.*, 2020, **187**, 188–193.
52 C. Oses, C. Toher and S. Curtarolo, High-entropy ceramics, *Nat. Rev. Mater.*, 2020, **5**, 295–309.
53 S. H. Shim, H. Pouraliakbar, Y. K. Kim, B. J. Lee, V. Fallah, Y.-K. Kim, K. R. Lim, Y.-S. Na and S. I. Hong, Exploring the impact of heat treatment on the transformation of hierarchical microstructure and mechanical properties in a non-equiatomic CrMnFeNiCu high-entropy alloy with a reversible structure, *J. Alloys Compd.*, 2023, **969**, 172514.
54 L. R. Owen, N. G. Jones, H. J. Stone and H. Y. Playford, Separation of static and dynamic displacements in the CrMnFeCoNi high entropy alloy, *Acta Mater.*, 2024, **262**, 119164.
55 Y.-Z. Wang and Y.-J. Wang, Disentangling diffusion heterogeneity in high-entropy alloys, *Acta Mater.*, 2022, **224**, 117527.
56 R. Wang, Y. Tang, S. Li, Y. Ai, Y. Li, B. Xiao, L. Zhu, X. Liu and S. Bai, Effect of lattice distortion on the diffusion behavior of high-entropy alloys, *J. Alloys Compd.*, 2020, **825**, 154099.

Published on 06 May 2025. Downloaded on 8/5/2025 11:23:10 AM.

57 L. Wang, L. Zhang, X. Lu, F. Wu, X. Sun, H. Zhao and Q. Li, Surprising cocktail effect in high entropy alloys on catalyzing magnesium hydride for solid-state hydrogen storage, *Chem. Eng. J.*, 2023, **465**, 142766.
58 Z. Wang, X. Tan, Z. Ye, S. Chen, G. Li, Q. Wang and S. Yuan, High entropy materials: potential catalysts for electrochemical water splitting, *ACS Symp. Ser.*, 2024, **26**, 9569–9598.
59 Z. Gu, J. Guo, J. Cao, X. Wang, X. Zhao, X. Zheng, W. Li, Z. Sun, H. Liang and X. Wu, An Advanced High–Entropy Fluorophosphate Cathode for Sodium–Ion Batteries with Increased Working Voltage and Energy Density, *Adv. Mater.*, 2022, **34**, 2110108.
60 Y. Gao, Z. Song, H. Hu, J. Mei, R. Kang, X. Zhu, B. Yang, J. Shao, Z. Chen, F. Li, S. Zhang and X. Lou, Optimizing high-temperature energy storage in tungsten bronze-structured ceramics via high-entropy strategy and bandgap engineering, *Nat. Commun.*, 2024, **15**, 5869.
61 Z. Wang, J. Li, S. Yuan, J. Yang, Z. Jin, X. Tan, J. Dang, W. Mu, G. Li and Q. Wang, Sabatier principle based design of high performance FeCoNiMnMoP high entropy electrocatalysis for alkaline water splitting, *Chem. Eng. J.*, 2024, **497**, 154650.
62 Z. W. Chen, J. Li, P. Ou, J. E. Huang, Z. Wen, L. Chen, X. Yao, G. Cai, C. C. Yang, C. V. Singh and Q. Jiang, Unusual Sabatier principle on high entropy alloy catalysts for hydrogen evolution reactions, *Nat. Commun.*, 2024, **15**, 359.
63 A. B. Laursen, R. B. Wexler, M. J. Whitaker, E. J. Izett, K. U. D. Calvinho, S. Hwang, R. Rucker, H. Wang, J. Li, E. Garfunkel, M. Greenblatt, A. M. Rappe and G. C. Dismukes, Climbing the Volcano of Electrocatalytic Activity while Avoiding Catalyst Corrosion: $Ni_3P$, a Hydrogen Evolution Electrocatalyst Stable in Both Acid and Alkali, *ACS Catal.*, 2018, **8**, 4408–4419.
64 M. Sheng, B. Jiang, B. Wu, F. Liao, X. Fan, H. Lin, Y. Li, Y. Lifshitz, S.-T. Lee and M. Shao, Approaching the Volcano Top: Iridium/Silicon Nanocomposites as Efficient Electrocatalysts for the Hydrogen Evolution Reaction, *ACS Nano*, 2019, **13**, 2786–2794.
65 X. Zhang, Y. Xu, M. Wang, E. Liu, N. Zhao, C. Shi, D. Lin, F. Zhu and C. He, A powder-metallurgy-based strategy toward three-dimensional graphene-like network for reinforcing copper matrix composites, *Nat. Commun.*, 2020, **11**, 2775.
66 L. Chen, Z. Li, P. Dai, P. Fu, Q. Tang and J. Chen, Microstructure and tensile properties of metastable Fe50Mn30Co10Cr10 high-entropy alloy prepared via powder metallurgy, *J. Alloys Compd.*, 2023, **955**, 170225.
67 A. Liang, D. C. Goodelman, A. M. Hodge, D. Farkas and P. S. Branicio, CoFeNiTi and CrFeNiTi high entropy alloy thin films microstructure formation, *Acta Mater.*, 2023, **257**, 119163.
68 Y. Xing, C. J. Li, Y. K. Mu, Y. D. Jia, K. K. Song, J. Tan, G. Wang, Z. Q. Zhang, J. H. Yi and J. Eckert, Strengthening and deformation mechanism of high-strength CrMnFeCoNi high entropy alloy prepared by powder metallurgy, *J. Mater. Sci. Technol.*, 2023, **132**, 119–131.
69 P. Pradhan, Powder metallurgical processing of CrMnFeCoMo high entropy alloy_ Phase evolution, microstructure, thermal stability and mechanical properties, *J. Alloys Compd.*, 2023, **969**, 172514.
70 J. He, Y. Qiao, R. Wang, Y. Tang, S. Li, X. Liu, Y. Ye, L. Zhu, Z. Wang and S. Bai, State and effect of oxygen on high entropy alloys prepared by powder metallurgy, *J. Alloys Compd.*, 2022, **891**, 161963.
71 H. Liu, H. Qin, J. Kang, L. Ma, G. Chen, Q. Huang, Z. Zhang, E. Liu, H. Lu, J. Li and N. Zhao, A freestanding nanoporous NiCoFeMoMn high-entropy alloy as an efficient electrocatalyst for rapid water splitting, *Chem. Eng. J.*, 2022, **435**, 134898.
72 Z. Chen, T. Zhang, X. Gao, Y. Huang, X. Qin, Y. Wang, K. Zhao, X. Peng, C. Zhang, L. Liu, M. Zeng and H. Yu, Engineering Microdomains of Oxides in High–Entropy Alloy Electrodes toward Efficient Oxygen Evolution, *Adv. Mater.*, 2021, **33**, 2101845.
73 X. Liu, Y. Duan, Y. Guo, H. Pang, Z. Li, X. Sun and T. Wang, Microstructure Design of High-Entropy Alloys Through a Multistage Mechanical Alloying Strategy for Temperature-Stable Megahertz Electromagnetic Absorption, *Nano-Micro Lett.*, 2022, **14**, 142.
74 S. Wang, B. Xu, W. Huo, H. Feng, X. Zhou, F. Fang, Z. Xie, J. K. Shang and J. Jiang, Efficient FeCoNiCuPd thin-film electrocatalyst for alkaline oxygen and hydrogen evolution reactions, *Appl. Catal., B*, 2022, **313**, 121472.
75 Y. Chida, T. Tomimori, T. Ebata, N. Taguchi, T. Ioroi, K. Hayashi, N. Todoroki and T. Wadayama, Experimental study platform for electrocatalysis of atomic-level controlled high-entropy alloy surfaces, *Nat. Commun.*, 2023, **14**, 4492.
76 K. Gu, D. Wang, C. Xie, T. Wang, G. Huang, Y. Liu, Y. Zou, L. Tao and S. Wang, Defect-Rich High-Entropy Oxide Nanosheets for Efficient 5- Hydroxymethylfurfural Electrooxidation, *Angew. Chem., Int. Ed.*, 2021, **60**, 20253–20258.
77 Y. Sun, W. Zhang, Q. Zhang, Y. Li, L. Gu and S. Guo, A general approach to high-entropy metallic nanowire electrocatalysts, *Matter*, 2023, **6**, 193–205.
78 Y. Huo, S. Xiu, L.-Y. Meng and B. Quan, Solvothermal synthesis and applications of micro/nano carbons: A review, *Chem. Eng. J.*, 2023, **451**, 138572.
79 L. Li, X. Liu, G. Wang, Y. Liu, W. Kang, N. Deng, X. Zhuang and X. Zhou, Research progress of ultrafine alumina fiber prepared by sol-gel method: A review, *Chem. Eng. J.*, 2021, **421**, 127744.
80 M. H. Mruthunjayappa, New prospects on solvothermal carbonisation assisted by organic solvents, ionic liquids and eutectic mixtures – A critical review, *Prog. Mater. Sci.*, 2022, **126**, 100932.
81 N. L. N. Broge, A. D. Bertelsen, F. Søndergaard-Pedersen and B. B. Iversen, Facile Solvothermal Synthesis of Pt–Ir–

 This journal is © the Partner Organisations 2025

Published on 06 May 2025. Downloaded on 8/5/2025 11:23:10 AM.

Pd–Rh–Ru–Cu–Ni–Co High-Entropy Alloy Nanoparticles, *Chem. Mater.*, 2023, **35**, 144–153.

82 S. Wang, W. Huo, F. Fang, Z. Xie, J. K. Shang and J. Jiang, High entropy alloy/C nanoparticles derived from polymetallic MOF as promising electrocatalysts for alkaline oxygen evolution reaction, *Chem. Eng. J.*, 2022, **429**, 132410.

83 L. Tang, Y. Yang, H. Guo, Y. Wang, M. Wang, Z. Liu, G. Yang, X. Fu, Y. Luo, C. Jiang, Y. Zhao, Z. Shao and Y. Sun, High Configuration Entropy Activated Lattice Oxygen for $O_2$ Formation on Perovskite Electrocatalyst, *Adv. Funct. Mater.*, 2022, **32**, 2112157.

84 K. Miao, W. Jiang, Z. Chen, Y. Luo, D. Xiang, C. Wang and X. Kang, Hollow–Structured and Polyhedron–Shaped High Entropy Oxide toward Highly Active and Robust Oxygen Evolution Reaction in a Full pH Range, *Adv. Mater.*, 2024, **36**, 2308490.

85 Y. Yao, Z. Huang, L. A. Hughes, J. Gao, T. Li, D. Morris, S. E. Zeltmann, B. H. Savitzky, C. Ophus, Y. Z. Finfrock, Q. Dong, M. Jiao, Y. Mao, M. Chi, P. Zhang, J. Li, A. M. Minor, R. Shahbazian-Yassar and L. Hu, Extreme mixing in nanoscale transition metal alloys, *Matter*, 2021, **4**, 2340–2353.

86 A. Abdelhafiz, B. Wang, A. R. Harutyunyan and J. Li, Carbothermal Shock Synthesis of High Entropy Oxide Catalysts: Dynamic Structural and Chemical Reconstruction Boosting the Catalytic Activity and Stability toward Oxygen Evolution Reaction, *Adv. Energy Mater.*, 2022, **12**, 2200742.

87 R. Rawat, B. K. Singh, A. Tiwari, N. Arun, A. P. Pathak, Y. Shadangi, N. K. Mukhopadhyay, S. R. Nelamarri, S. V. Rao and A. Tripathi, Formation of Cu-Ni enriched phases during laser processing of non-equiatomic AlSiCrMnFeNiCu high entropy alloy nanoparticles, *J. Alloys Compd.*, 2022, **927**, 166905.

88 A. D. Pendergast, M. W. Glasscott, C. Renault and J. E. Dick, One-step electrodeposition of ligand-free PdPt alloy nanoparticles from water droplets: Controlling size, coverage, and elemental stoichiometry, *Electrochem. Commun.*, 2019, **98**, 1–5.

89 S. Gao, S. Hao, Z. Huang, Y. Yuan, S. Han, L. Lei, X. Zhang, R. Shahbazian-Yassar and J. Lu, Synthesis of high-entropy alloy nanoparticles on supports by the fast moving bed pyrolysis, *Nat. Commun.*, 2020, **11**, 2016.

90 B. Wang, C. Wang, X. Yu, Y. Cao, L. Gao, C. Wu, Y. Yao, Z. Lin and Z. Zou, General synthesis of high-entropy alloy and ceramic nanoparticles in nanoseconds, *Nat. Synth.*, 2022, **1**, 138–146.

91 M. W. Glasscott, A. D. Pendergast, S. Goines, A. R. Bishop, A. T. Hoang, C. Renault and J. E. Dick, Electrosynthesis of high-entropy metallic glass nanoparticles for designer, multi-functional electrocatalysis, *Nat. Commun.*, 2019, **10**, 2650.

92 S.-Q. Chang, C.-C. Cheng, P.-Y. Cheng, C.-L. Huang and S.-Y. Lu, Pulse electrodeposited FeCoNiMnW high entropy alloys as efficient and stable bifunctional electrocatalysts for acidic water splitting, *Chem. Eng. J.*, 2022, **446**, 137452.

93 Q. Liu, Y. Zhao, H. Pan, J. Wang, K. Sun and F. Gao, A fine 3d transition metal regulation strategy toward high-entropy alloy mesoporous nanotubes as efficient electrocatalysts, *Chem. Eng. J.*, 2023, **477**, 147099.

94 J. Wordsworth, T. M. Benedetti, S. V. Somerville, W. Schuhmann, R. D. Tilley and J. J. Gooding, The Influence of Nanoconfinement on Electrocatalysis, *Angew. Chem., Int. Ed.*, 2022, **61**, e202200755.

95 L. Zhang, W. Cai and N. Bao, Top–Level Design Strategy to Construct an Advanced High–Entropy Co–Cu–Fe–Mo (Oxy) Hydroxide Electrocatalyst for the Oxygen Evolution Reaction, *Adv. Mater.*, 2021, **33**, 2100745.

96 A. J. Cohen, P. Mori-Sánchez and W. Yang, Challenges for Density Functional Theory, *Chem. Rev.*, 2012, **112**, 289–320.

97 Q. Wang, L. Velasco, B. Breitung and V. Presser, High–Entropy Energy Materials in the Age of Big Data: A Critical Guide to Next–Generation Synthesis and Applications, *Adv. Energy Mater.*, 2021, **11**, 2102355.

98 X. Liao, R. Lu, L. Xia, Q. Liu, H. Wang, K. Zhao, Z. Wang and Y. Zhao, Density Functional Theory for Electrocatalysis, *Energy Environ. Mater.*, 2022, **5**, 157–185.

99 P. Zimmermann, S. Peredkov, P. M. Abdala, S. DeBeer, M. Tromp, C. Müller and J. A. Van Bokhoven, Modern X-ray spectroscopy: XAS and XES in the laboratory, *Coord. Chem. Rev.*, 2020, **423**, 213466.

100 D. Wang, Z. Chen, Y. Wu, Y. Huang, L. Tao, J. Chen, C. Dong, C. V. Singh and S. Wang, Structurally ordered high–entropy intermetallic nanoparticles with enhanced C–C bond cleavage for ethanol oxidation, *SmartMat*, 2023, **4**, 1–11.

101 K. Zeng, J. Zhang, W. Gao, L. Wu, H. Liu, J. Gao, Z. Li, J. Zhou, T. Li, Z. Liang, B. Xu and Y. Yao, Surface–Decorated High–Entropy Alloy Catalysts with Significantly Boosted Activity and Stability, *Adv. Funct. Mater.*, 2022, **32**, 2204643.

102 H. Minamihara, K. Kusada, D. Wu, T. Yamamoto, T. Toriyama, S. Matsumura, L. S. R. Kumara, K. Ohara, O. Sakata, S. Kawaguchi, Y. Kubota and H. Kitagawa, Continuous-Flow Reactor Synthesis for Homogeneous 1 nm-Sized Extremely Small High-Entropy Alloy Nanoparticles, *J. Am. Chem. Soc.*, 2022, **144**(26), 11525–11529.

103 C. Luan, D. Escalera-López, U. Hagemann, A. Kostka, G. Laplanche, D. Wu, S. Cherevko and T. Li, Revealing Dynamic Surface and Subsurface Reconstruction of High-Entropy Alloy Electrocatalysts during the Oxygen Evolution Reaction at the Atomic Scale, *ACS Catal.*, 2024, **14**, 12704–12716.

104 L. Su, X. Chen, L. Xu, T. Eldred, J. Smith, C. DellaRova, H. Wang and W. Gao, Visualizing the Formation of High-Entropy Fluorite Oxides from an Amorphous Precursor at Atomic Resolution, *ACS Nano*, 2022, **16**, 21397–21406.

Published on 06 May 2025. Downloaded on 8/5/2025 11:23:10 AM.

105 H. Xu, Z. Zhang, J. Liu, C.-L. Do-Thanh, H. Chen, S. Xu, Q. Lin, Y. Jiao, J. Wang, Y. Wang, Y. Chen and S. Dai, Entropy-stabilized single-atom Pd catalysts via high-entropy fluorite oxide supports, *Nat. Commun.*, 2020, **11**, 3908.

106 J. Ding, D. Wu, J. Zhu, S. Huang, F. Rodríguez-Hernández, Y. Chen, C. Lu, S. Zhou, J. Zhang, D. Tranca and X. Zhuang, High-entropy carbons: From high-entropy aromatic species to single-atom catalysts for electrocatalysis, *Chem. Eng. J.*, 2021, **426**, 131320.

107 Y. Yao, Q. Dong, A. Brozena, J. Luo, J. Miao, M. Chi, C. Wang, I. G. Kevrekidis, Z. J. Ren, J. Greeley, G. Wang, A. Anapolsky and L. Hu, High-entropy nanoparticles: Synthesis-structure-property relationships and data-driven discovery, *Sci*, 2022, **376**, eabn3103.

108 K. Kaufmann, D. Maryanovsky, W. M. Mellor, C. Zhu, A. S. Rosengarten, T. J. Harrington, C. Oses, C. Toher, S. Curtarolo and K. S. Vecchio, Discovery of high-entropy ceramics via machine learning, *npj Comput. Mater.*, 2020, **6**, 42.

109 Y. Ikeda, B. Grabowski and F. Körmann, Ab initio phase stabilities and mechanical properties of multicomponent alloys: A comprehensive review for high entropy alloys and compositionally complex alloys, *Mater. Charact.*, 2019, **147**, 464–511.

110 R. Wang, J. Huang, X. Zhang, J. Han, Z. Zhang, T. Gao, L. Xu, S. Liu, P. Xu and B. Song, Two-Dimensional High-Entropy Metal Phosphorus Trichalcogenides for Enhanced Hydrogen Evolution Reaction, *ACS Nano*, 2022, **16**, 3593–3603.

111 H. Li, Y. Han, H. Zhao, W. Qi, D. Zhang, Y. Yu, W. Cai, S. Li, J. Lai, B. Huang and L. Wang, Fast site-to-site electron transfer of high-entropy alloy nanocatalyst driving redox electrocatalysis, *Nat. Commun.*, 2020, **11**, 5437.

112 D. Strmcnik, P. P. Lopes, B. Genorio, V. R. Stamenkovic and N. M. Markovic, Design principles for hydrogen evolution reaction catalyst materials, *Nano Energy*, 2016, **29**, 29–36.

113 I. T. McCrum and M. T. M. Koper, The role of adsorbed hydroxide in hydrogen evolution reaction kinetics on modified platinum, *Nat. Energy*, 2020, **5**, 891–899.

114 X. Wang, Y. Zheng, W. Sheng, Z. J. Xu, M. Jaroniec and S.-Z. Qiao, Strategies for design of electrocatalysts for hydrogen evolution under alkaline conditions, *Mater. Today*, 2020, **36**, 125–138.

115 X. Zou and Y. Zhang, Noble metal-free hydrogen evolution catalysts for water splitting, *Chem. Soc. Rev.*, 2015, **44**, 5148–5180.

116 C. Hu, L. Zhang and J. Gong, Recent progress made in the mechanism comprehension and design of electrocatalysts for alkaline water splitting, *Energy Environ. Sci.*, 2019, **12**, 2620–2645.

117 D. Liu, G. Xu, H. Yang, H. Wang and B. Y. Xia, Rational Design of Transition Metal Phosphide–Based Electrocatalysts for Hydrogen Evolution, *Adv. Funct. Mater.*, 2023, **33**, 2208358.

118 P. Zhu, X. Xiong and D. Wang, Regulations of active moiety in single atom catalysts for electrochemical hydrogen evolution reaction, *Nano Res.*, 2022, **15**, 5792–5815.

119 S. Anantharaj, S. Noda, V. R. Jothi, S. Yi, M. Driess and P. W. Menezes, Strategies and Perspectives to Catch the Missing Pieces in Energy–Efficient Hydrogen Evolution Reaction in Alkaline Media, *Angew. Chem., Int. Ed.*, 2021, **60**, 18981–19006.

120 W. Yang and S. Chen, Recent progress in electrode fabrication for electrocatalytic hydrogen evolution reaction: A mini review, *Chem. Eng. J.*, 2020, **393**, 124726.

121 Z. Wang, B. Xiao, Z. Lin, Y. Xu, Y. Lin, F. Meng, Q. Zhang, L. Gu, B. Fang, S. Guo and W. Zhong, $PtSe_2$/Pt Heterointerface with Reduced Coordination for Boosted Hydrogen Evolution Reaction, *Angew. Chem., Int. Ed.*, 2021, **60**, 23388–23393.

122 H. Wu, C. Feng, L. Zhang, J. Zhang and D. P. Wilkinson, Non-noble Metal Electrocatalysts for the Hydrogen Evolution Reaction in Water Electrolysis, *Electrochem. Energy Rev.*, 2021, **4**, 473–507.

123 J. Gu, L. Li, Y. Xie, B. Chen, F. Tian, Y. Wang, J. Zhong, J. Shen and J. Lu, Turing structuring with multiple nanotwins to engineer efficient and stable catalysts for hydrogen evolution reaction, *Nat. Commun.*, 2023, **14**, 5389.

124 R. Li, X. Liu, W. Liu, Z. Li, K. C. Chan and Z. Lu, Design of Hierarchical Porosity Via Manipulating Chemical and Microstructural Complexities in High–Entropy Alloys for Efficient Water Electrolysis, *Adv. Sci.*, 2022, **9**, 2105808.

125 G. Feng, Y. Pan, D. Su and D. Xia, Constructing Fully–Active and Ultra–Active Sites in High–Entropy Alloy Nanoclusters for Hydrazine Oxidation–Assisted Electrolytic Hydrogen Production, *Adv. Mater.*, 2024, **36**, 2309715.

126 H. Li, H. Zhu, Q. Shen, S. Huang, S. Lu, P. Ma, W. Dong and M. Du, A novel synergistic confinement strategy for controlled synthesis of high-entropy alloy electrocatalysts, *Chem. Commun.*, 2021, **57**, 2637–2640.

127 D. Zhang, Y. Shi, H. Zhao, W. Qi, X. Chen, T. Zhan, S. Li, B. Yang, M. Sun, J. Lai, B. Huang and L. Wang, The facile oil-phase synthesis of a multi-site synergistic high-entropy alloy to promote the alkaline hydrogen evolution reaction, *J. Mater. Chem. A*, 2021, **9**, 889–893.

128 T. Yu, Y. Zhang, Y. Hu, K. Hu, X. Lin, G. Xie, X. Liu, K. M. Reddy, Y. Ito and H.-J. Qiu, Twelve-Component Free-Standing Nanoporous High-Entropy Alloys for Multifunctional Electrocatalysis, *ACS Mater. Lett.*, 2022, **4**, 181–189.

129 Q. Chen, X. Han, Z. Xu, Q. Chen, Q. Wu, T. Zheng, P. Wang, Z. Wang, J. Wang, H. Li, Z. Xia and J. Hao, Atomic phosphorus induces tunable lattice strain in high entropy alloys and boosts alkaline water splitting, *Nano Energy*, 2023, **110**, 108380.

130 M. Wei, Y. Sun, F. Ai, S. Xi, J. Zhang and J. Wang, Stretchable high-entropy alloy nanoflowers enable enhanced alkaline hydrogen evolution catalysis, *Appl. Catal., B*, 2023, **334**, 122814.

 This journal is © the Partner Organisations 2025

Published on 06 May 2025. Downloaded on 8/5/2025 11:23:10 AM.

131 Y. Lei, L. Zhang, W. Xu, C. Xiong, W. Chen, X. Xiang, B. Zhang and H. Shang, Carbon-supported high-entropy Co-Zn-Cd-Cu-Mn sulfide nanoarrays promise high-performance overall water splitting, *Nano Res.*, 2022, **15**, 6054–6061.

132 K. Li, J. He, X. Guan, Y. Tong, Y. Ye, L. Chen and P. Chen, Phosphorus–Modified Amorphous High–Entropy CoFeNiCrMn Compound as High–Performance Electrocatalyst for Hydrazine–Assisted Water Electrolysis, *Small*, 2023, **19**, 2302130.

133 R. Yao, Y. Zhou, H. Shi, W. Wan, Q. Zhang, L. Gu, Y. Zhu, Z. Wen, X. Lang and Q. Jiang, Nanoporous Surface High–Entropy Alloys as Highly Efficient Multisite Electrocatalysts for Nonacidic Hydrogen Evolution Reaction, *Adv. Funct. Mater.*, 2021, **31**, 2009613.

134 Z.-X. Cai, H. Goou, Y. Ito, T. Tokunaga, M. Miyauchi, H. Abe and T. Fujita, Nanoporous ultra-high-entropy alloys containing fourteen elements for water splitting electrocatalysis, *Chem. Sci.*, 2021, **12**, 11306–11315.

135 M. Wei, Y. Sun, J. Zhang, F. Ai, S. Xi and J. Wang, High-entropy alloy nanocrystal assembled by nanosheets with d–d electron interaction for hydrogen evolution reaction, *Energy Environ. Sci.*, 2023, **16**, 4009–4019.

136 D. Wu, K. Kusada, T. Yamamoto, T. Toriyama, S. Matsumura, I. Gueye, O. Seo, J. Kim, S. Hiroi, O. Sakata, S. Kawaguchi, Y. Kubota and H. Kitagawa, On the electronic structure and hydrogen evolution reaction activity of platinum group metal-based high-entropy-alloy nanoparticles, *Chem. Sci.*, 2020, **11**, 12731–12736.

137 Y. Wang, N. Gong, H. Liu, W. Ma, K. Hippalgaonkar, Z. Liu and Y. Huang, Ordering–Dependent Hydrogen Evolution and Oxygen Reduction Electrocatalysis of High–Entropy Intermetallic Pt $_4$ FeCoCuNi, *Adv. Mater.*, 2023, **35**, 2302067.

138 Z. Jia, T. Yang, L. Sun, Y. Zhao, W. Li, J. Luan, F. Lyu, L. Zhang, J. J. Kruzic, J. Kai, J. C. Huang, J. Lu and C. T. Liu, A Novel Multinary Intermetallic as an Active Electrocatalyst for Hydrogen Evolution, *Adv. Mater.*, 2020, **32**, 2000385.

139 J. Hao, Z. Zhuang, K. Cao, G. Gao, C. Wang, F. Lai, S. Lu, P. Ma, W. Dong, T. Liu, M. Du and H. Zhu, Unraveling the electronegativity-dominated intermediate adsorption on high-entropy alloy electrocatalysts, *Nat. Commun.*, 2022, **13**, 2662.

140 G. Feng, F. Ning, J. Song, H. Shang, K. Zhang, Z. Ding, P. Gao, W. Chu and D. Xia, Sub-2 nm Ultrasmall High-Entropy Alloy Nanoparticles for Extremely Superior Electrocatalytic Hydrogen Evolution, *J. Am. Chem. Soc.*, 2021, **143**, 17117–17127.

141 X. Cui, Y. Liu, X. Wang, X. Tian, Y. Wang, G. Zhang, T. Liu, J. Ding, W. Hu and Y. Chen, Rapid High-Temperature Liquid Shock Synthesis of High-Entropy Alloys for Hydrogen Evolution Reaction, *ACS Nano*, 2024, **18**, 2948–2957.

142 X. Li, Z. Cheng and X. Wang, Understanding the Mechanism of the Oxygen Evolution Reaction with Consideration of Spin, *Electrochem. Energy Rev.*, 2021, **4**, 136–145.

143 L. Gao, X. Cui, C. D. Sewell, J. Li and Z. Lin, Recent advances in activating surface reconstruction for the high-efficiency oxygen evolution reaction, *Chem. Soc. Rev.*, 2021, **50**, 8428–8469.

144 X. Xie, L. Du, L. Yan, S. Park, Y. Qiu, J. Sokolowski, W. Wang and Y. Shao, Oxygen Evolution Reaction in Alkaline Environment: Material Challenges and Solutions, *Adv. Funct. Mater.*, 2022, **32**, 2110036.

145 Z. Shi, X. Wang, J. Ge, C. Liu and W. Xing, Fundamental understanding of the acidic oxygen evolution reaction: mechanism study and state-of-the-art catalysts, *Nanoscale*, 2020, **12**, 13249–13275.

146 F.-Y. Chen, Z.-Y. Wu, Z. Adler and H. Wang, Stability challenges of electrocatalytic oxygen evolution reaction: From mechanistic understanding to reactor design, *Joule*, 2021, **5**, 1704–1731.

147 C. Lee, K. Shin, Y. Park, Y. H. Yun, G. Doo, G. H. Jung, M. Kim, W. Cho, C. Kim, H. M. Lee, H. Y. Kim, S. Lee, G. Henkelman and H. Cho, Catalyst–Support Interactions in $Zr_2$ $ON_2$ –Supported $IrO_x$ Electrocatalysts to Break the Trade–Off Relationship Between the Activity and Stability in the Acidic Oxygen Evolution Reaction, *Adv. Funct. Mater.*, 2023, **33**, 2301557.

148 Y. Mei, Y. Feng, C. Zhang, Y. Zhang, Q. Qi and J. Hu, High-Entropy Alloy with Mo-Coordination as Efficient Electrocatalyst for Oxygen Evolution Reaction, *ACS Catal.*, 2022, **12**, 10808–10817.

149 J. Tang, J. L. Xu, Z. G. Ye, X. B. Li and J. M. Luo, Microwave sintered porous CoCrFeNiMo high entropy alloy as an efficient electrocatalyst for alkaline oxygen evolution reaction, *J. Mater. Sci. Technol.*, 2021, **79**, 171–177.

150 Z. Jia, K. Nomoto, Q. Wang, C. Kong, L. Sun, L. Zhang, S. Liang, J. Lu and J. J. Kruzic, A Self–Supported High–Entropy Metallic Glass with a Nanosponge Architecture for Efficient Hydrogen Evolution under Alkaline and Acidic Conditions, *Adv. Funct. Mater.*, 2021, **31**, 2101586.

151 Q. Wang, J. Li, Y. Li, G. Shao, Z. Jia and B. Shen, Non-noble metal-based amorphous high-entropy oxides as efficient and reliable electrocatalysts for oxygen evolution reaction, *Nano Res.*, 2022, **15**, 8751–8759.

152 H. Qiao, X. Wang, Q. Dong, H. Zheng, G. Chen, M. Hong, C.-P. Yang, M. Wu, K. He and L. Hu, A high-entropy phosphate catalyst for oxygen evolution reaction, *Nano Energy*, 2021, **86**, 106029.

153 Q. Wang, Z. Jia, J. Li, Y. He, Y. Yang, Y. Li, L. Sun and B. Shen, Attractive Electron Delocalization Behavior of FeCoMoPB Amorphous Nanoplates for Highly Efficient Alkaline Water Oxidation, *Small*, 2022, **18**, 2204135.

154 L. Yi, S. Xiao, Y. Wei, D. Li, R. Wang, S. Guo and W. Hu, Free-standing high-entropy alloy plate for efficient water oxidation catalysis: structure/composition evolution and implication of high-valence metals, *Chem. Eng. J.*, 2023, **469**, 144015.

Published on 06 May 2025. Downloaded on 8/5/2025 11:23:10 AM.

155 Y. Sun, W. Wu, L. Yu, S. Xu, Y. Zhang, L. Yu, B. Xia, S. Ding, M. Li, L. Jiang, J. Duan, J. Zhu and S. Chen, Asymmetric acidic/alkaline $N_2$ electrofixation accelerated by high–entropy metal–organic framework derivatives, *Carbon Energy*, 2023, **5**, e263.

156 C. Triolo, K. Moulaee, A. Ponti, G. Pagot, V. Di Noto, N. Pinna, G. Neri and S. Santangelo, Spinel–Structured High–Entropy Oxide Nanofibers as Electrocatalysts for Oxygen Evolution in Alkaline Solution: Effect of Metal Combination and Calcination Temperature, *Adv. Funct. Mater.*, 2024, **34**, 2306375.

157 S. Jo, M. Kim, K. B. Lee, H. Choi, L. Zhang and J. I. Sohn, Nonprecious High–Entropy Chalcogenide Glasses–Based Electrocatalysts for Efficient and Stable Acidic Oxygen Evolution Reaction in Proton Exchange Membrane Water Electrolysis, *Adv. Energy Mater.*, 2023, **13**, 2301420.

158 M. Han, C. Wang, J. Zhong, J. Han, N. Wang, A. Seifitokaldani, Y. Yu, Y. Liu, X. Sun, A. Vomiero and H. Liang, Promoted self-construction of β-NiOOH in amorphous high entropy electrocatalysts for the oxygen evolution reaction, *Appl. Catal., B*, 2022, **301**, 120764.

159 Y. Cui, S. Jiang, Q. Fu, R. Wang, P. Xu, Y. Sui, X. Wang, Z. Ning, J. Sun, X. Sun, A. Nikiforov and B. Song, Cost–Effective High Entropy Core–Shell Fiber for Stable Oxygen Evolution Reaction at 2 A $cm^{-2}$, *Adv. Funct. Mater.*, 2023, **33**, 2306889.

160 Q. Zhang, Y. Hu, H. Wu, X. Zhao, M. Wang, S. Wang, R. Feng, Q. Chen, F. Song, M. Chen and P. Liu, Entropy-Stabilized Multicomponent Porous Spinel Nanowires of NiFeXO4 (X = Fe, Ni, Al, Mo, Co, Cr) for Efficient and Durable Electrocatalytic Oxygen Evolution Reaction in Alkaline Medium, *ACS Nano*, 2023, **17**, 1485–1494.

161 Z. Jin, X. Zhou, Y. Hu, X. Tang, K. Hu, K. M. Reddy, X. Lin and H.-J. Qiu, A fourteen-component high-entropy alloy@-oxide bifunctional electrocatalyst with a record-low Δ *E* of 0.61 V for highly reversible Zn–air batteries, *Chem. Sci.*, 2022, **13**, 12056–12064.

162 L.-H. Liu, N. Li, M. Han, J.-R. Han and H.-Y. Liang, Scalable synthesis of nanoporous high entropy alloys for electrocatalytic oxygen evolution, *Rare Met.*, 2022, **41**, 125–131.

163 H. Zhu, S. Sun, J. Hao, Z. Zhuang, S. Zhang, T. Wang, Q. Kang, S. Lu, X. Wang, F. Lai, T. Liu, G. Gao, M. Du and D. Wang, A high-entropy atomic environment converts inactive to active sites for electrocatalysis, *Energy Environ. Sci.*, 2023, **16**, 619–628.

164 W. Hooch Antink, S. Lee, H. S. Lee, H. Shin, T. Y. Yoo, W. Ko, J. Shim, G. Na, Y. Sung and T. Hyeon, High–Valence Metal–Driven Electronic Modulation for Boosting Oxygen Evolution Reaction in High–Entropy Spinel Oxide, *Adv. Funct. Mater.*, 2024, **34**, 2309438.

165 Z. Gao, J.-H. Liu, S. Wang, W. Yang, W. Wang, L. Li, H. Guo, J. Zheng, S. Ramakrishna, J. Zhang, L. Yang and Y.-Z. Long, Quenching controlled spin exchange interactions and spin selective electron transfer for oxygen evolution reactions, *Chem. Eng. J.*, 2024, **496**, 154216.

166 L. He, H. Kang, G. Hou, X. Qiao, X. Jia, W. Qin and X. Wu, Low-temperature synthesis of nano-porous high entropy spinel oxides with high grain boundary density for oxygen evolution reaction, *Chem. Eng. J.*, 2023, **460**, 141675.

167 X. F. Lu, B. Y. Xia, S. Zang and X. W. (. Lou, Metal–Organic Frameworks Based Electrocatalysts for the Oxygen Reduction Reaction, *Angew. Chem.*, 2020, **132**, 4662–4678.

168 J. Zhang, H. Yang and B. Liu, Coordination Engineering of Single–Atom Catalysts for the Oxygen Reduction Reaction: A Review, *Adv. Energy Mater.*, 2021, **11**, 2002473.

169 Y. Zhao, D. P. A. Saseendran, C. Huang, C. A. Triana, W. R. Marks, H. Chen, H. Zhao and G. R. Patzke, Oxygen Evolution/Reduction Reaction Catalysts: From In Situ Monitoring and Reaction Mechanisms to Rational Design, *Chem. Rev.*, 2023, **123**, 6257–6358.

170 X. Tian, X. F. Lu, B. Y. Xia and X. W. Lou, Advanced Electrocatalysts for the Oxygen Reduction Reaction in Energy Conversion Technologies, *Joule*, 2020, **4**, 45–68.

171 Z. Liang, H. Guo, G. Zhou, K. Guo, B. Wang, H. Lei, W. Zhang, H. Zheng, U. Apfel and R. Cao, Metal–Organic–Framework–Supported Molecular Electrocatalysis for the Oxygen Reduction Reaction, *Angew. Chem.*, 2021, **133**, 8553–8557.

172 M. A. Ud Din, M. Idrees, S. Jamil, S. Irfan, G. Nazir, M. A. Mudassir, M. S. Saleem, S. Batool, N. Cheng and R. Saidur, Advances and challenges of methanol-tolerant oxygen reduction reaction electrocatalysts for the direct methanol fuel cell, *J. Energy Chem.*, 2023, **77**, 499–513.

173 R. He, L. Yang, Y. Zhang, D. Jiang, S. Lee, S. Horta, Z. Liang, X. Lu, A. Ostovari Moghaddam, J. Li, M. Ibáñez, Y. Xu, Y. Zhou and A. Cabot, A 3d–4d–5d High Entropy Alloy as a Bifunctional Oxygen Catalyst for Robust Aqueous Zinc–Air Batteries, *Adv. Mater.*, 2023, 2303719.

174 Z. Huang, Y. Peng, L. Xing, M. Xu, M. Fang, H. Xie, J. Li, Y. Zhou, P. Wu, N. Wang, C. Tang, M. Wu, L. Wang, S. Ye and L. Du, Microenvironment regulation to synthesize sub-3 nm Pt-based high-entropy alloy nanoparticles enabling compressed lattice to boost electrocatalysis, *Appl. Catal., B*, 2025, **363**, 124775.

175 X. Zou, X. Zhao, B. Pang, H. Ma, K. Zeng, S. Zhi and H. Guo, Interstitial Oxygen Acts as Electronic Buffer Stabilizing High–Entropy Alloys for Trifunctional Electrocatalysis, *Adv. Mater.*, 2024, **36**, 2412954.

176 X. Lei, Q. Tang, Y. Zheng, P. Kidkhunthod, X. Zhou, B. Ji and Y. Tang, High-entropy single-atom activated carbon catalysts for sustainable oxygen electrocatalysis, *Nat. Sustainable*, 2023, **6**, 816–826.

177 Z. Jin, J. Lyu, Y.-L. Zhao, H. Li, Z. Chen, X. Lin, G. Xie, X. Liu, J.-J. Kai and H.-J. Qiu, Top–Down Synthesis of Noble Metal Particles on High-Entropy Oxide Supports for Electrocatalysis, *Chem. Mater.*, 2021, **33**, 1771–1780.

178 G. Feng, F. Ning, Y. Pan, T. Chen and D. Xia, Engineering Structurally Ordered High-Entropy Intermetallic Nanoparticles with High-Activity Facets for Oxygen Reduction in Practical Fuel Cells, *J. Am. Chem. Soc.*, 2023, **145**(20), 11140–11150.

 This journal is © the Partner Organisations 2025

Published on 06 May 2025. Downloaded on 8/5/2025 11:23:10 AM.

179 Z. Qiu, X. Guo, S. Cao, M. Du, Q. Wang, Y. Pi and H. Pang, High–Entropy Ag–Ru–Based Electrocatalysts with Dual–Active–Center for Highly Stable Ultra–Low–Temperature Zinc–Air Batteries, *Angew. Chem., Int. Ed.*, 2024, e202415216.

180 G. Zhu, Y. Jiang, H. Yang, H. Wang, Y. Fang, L. Wang, M. Xie, P. Qiu and W. Luo, Constructing Structurally Ordered High–Entropy Alloy Nanoparticles on Nitrogen–Rich Mesoporous Carbon Nanosheets for High–Performance Oxygen Reduction, *Adv. Mater.*, 2022, **34**, 2110128.

181 Q. Zhang, T. Shen, M. Song, S. Wang, J. Zhang, X. Huang, S. Lu and D. Wang, High-entropy L12-Pt(FeCoNiCuZn)3 intermetallics for ultrastable oxygen reduction reaction, *J. Energy Chem.*, 2023, **86**, 158–166.

182 R. He, L. Yang, Y. Zhang, X. Wang, S. Lee, T. Zhang, L. Li, Z. Liang, J. Chen, J. Li, A. Ostovari Moghaddam, J. Llorca, M. Ibáñez, J. Arbiol, Y. Xu and A. Cabot, A CrMnFeCoNi high entropy alloy boosting oxygen evolution/reduction reactions and zinc-air battery performance, *Energy Storage Mater.*, 2023, **58**, 287–298.

183 Y. Wang, W. Luo, S. Gong, L. Luo, Y. Li, Y. Zhao and Z. Li, Synthesis of High–Entropy–Alloy Nanoparticles by a Step–Alloying Strategy as a Superior Multifunctional Electrocatalyst, *Adv. Mater.*, 2023, **35**, 2302499.

184 P. Rao, Y. Deng, W. Fan, J. Luo, P. Deng, J. Li, Y. Shen and X. Tian, Movable type printing method to synthesize high-entropy single-atom catalysts, *Nat. Commun.*, 2022, **13**, 5071.

185 Z. Jin, J. Lyu, Y.-L. Zhao, H. Li, X. Lin, G. Xie, X. Liu, J.-J. Kai and H.-J. Qiu, Rugged High-Entropy Alloy Nanowires with in Situ Formed Surface Spinel Oxide As Highly Stable Electrocatalyst in Zn–Air Batteries, *ACS Mater. Lett.*, 2020, **2**, 1698–1706.

186 W. Zhang, X. Feng, Z. X. Mao, J. Li and Z. Wei, Stably Immobilizing Sub–3 nm High–Entropy Pt Alloy Nanocrystals in Porous Carbon as Durable Oxygen Reduction Electrocatalyst, *Adv. Funct. Mater.*, 2022, **32**, 2204110.

187 M. Wu, M. Cui, L. Wu, S. Hwang, C. Yang, Q. Xia, G. Zhong, H. Qiao, W. Gan, X. Wang, D. Kline, M. R. Zachariah, D. Su, T. Li and L. Hu, Hierarchical Polyelemental Nanoparticles as Bifunctional Catalysts for Oxygen Evolution and Reduction Reactions, *Adv. Energy Mater.*, 2020, **10**, 2001119.

188 Y. Yao, Z. Huang, T. Li, H. Wang, Y. Liu, H. S. Stein, Y. Mao, J. Gao, M. Jiao, Q. Dong, J. Dai, P. Xie, H. Xie, S. D. Lacey, I. Takeuchi, J. M. Gregoire, R. Jiang, C. Wang, A. D. Taylor, R. Shahbazian-Yassar and L. Hu, High-throughput, combinatorial synthesis of multimetallic nanoclusters, *Proc. Natl. Acad. Sci. U. S. A.*, 2020, **117**, 6316–6322.

189 P. Zhang, X. Hui, Y. Nie, R. Wang, C. Wang, Z. Zhang and L. Yin, New Conceptual Catalyst on Spatial High–Entropy Alloy Heterostructures for High–Performance Li–$O_2$ Batteries, *Small*, 2023, **19**, 2206742.

190 Q. Zhang, Z. Zheng, R. Gao, X. Xiao, M. Jiao, B. Wang, G. Zhou and H. Cheng, Constructing Bipolar Dual–Active Sites through High–Entropy–Induced Electric Dipole Transition for Decoupling Oxygen Redox, *Adv. Mater.*, 2024, **36**, 2401018.

191 M. Khalid, M. A. K. Y. Shah, N. Akbar, N. Mushtaq, R. Raza, J. Wang and B. Zhu, High-Entropy Li-doped rock salt catalyst for low-Temperature ceramic fuel cells, *Fuel*, 2025, **379**, 133044.

192 K. Kang, Y. Liu, X. Liu, C. Wang and M. Wei, Local lattice distortion regulation in high entropy engineering to enhance the triple conductivity of layered Ruddlesden-Popper perovskite cathode in H+-SOFCs, *Chem. Eng. J.*, 2025, **507**, 159463.

193 D. Du, H. He, R. Zheng, L. Zeng, X. Wang, C. Shu and C. Zhang, Single–Atom Immobilization Boosting Oxygen Redox Kinetics of High–Entropy Perovskite Oxide Toward High–Performance Lithium–Oxygen Batteries, *Adv. Energy Mater.*, 2024, **14**, 2304238.

194 X. Xu, Z. Shao and S. P. Jiang, High–Entropy Materials for Water Electrolysis, *Energy Technol.*, 2022, **10**, 2200573.

195 J. Cha, S. Cho, D. Kim, D. Jeon, S. Park, J. Jung, I. Kim and S. Choi, Flash–Thermal Shock Synthesis of High–Entropy Alloys Toward High–Performance Water Splitting, *Adv. Mater.*, 2023, **35**, 2305222.

196 C. Feng, Y. Zhou, M. Chen, L. Zou, X. Li, X. An, Q. Zhao, P. Xiaokaiti, A. Abudula, K. Yan and G. Guan, High-entropy spinel (FeCoNiMnAl)3O4 with three-dimensional microflower structure for stable seawater oxidation, *Appl. Catal., B*, 2024, **349**, 123875.

197 C. E. Park, G. H. Jeong, V. Maheskumar, J. Theerthagiri and M. Y. Choi, *In situ* capturing site-to-site reactive species in $CO_2$ -laser-patterned high-entropy alloy nanoflowers for robust alkaline seawater electrolysis, *J. Mater. Chem. A*, 2024, **12**, 21744–21757.

198 Y. Xie, S. Xu, A. C. Meng, B. Zheng, Z. Chen, J. M. Tour and J. Lin, Laser-induced high-entropy alloys as long-duration bifunctional electrocatalysts for seawater splitting, *Energy Environ. Sci.*, 2024, **17**, 8670–8682.

199 Y. Zhai, X. Ren, B. Wang and S. Liu, High–Entropy Catalyst—A Novel Platform for Electrochemical Water Splitting, *Adv. Funct. Mater.*, 2022, **32**, 2207536.

200 Z. Qiu, Y. Li, Y. Gao, Z. Meng, Y. Sun, Y. Bai, N. Suen, H. Chen, Y. Pi and H. Pang, 2D MOF–assisted Pyrolysis–displacement–alloying Synthesis of High–entropy Alloy Nanoparticles Library for Efficient Electrocatalytic Hydrogen Oxidation, *Angew. Chem., Int. Ed.*, 2023, **62**, e202306881.